J. Phycol. 58, 465–486 (2022)

DOI: 10.1111/jpy.13245

# UNRAVELING THE *GONYAULAX BALTICA* SPECIES COMPLEX: CYST–THECA RELATIONSHIP OF *IMPAGIDINIUM VARIASEPTUM*, *SPINIFERITES PSEUDODELICATUS* SP. NOV. AND *S. RISTINGENSIS* (GONYAULACACEAE, DINOPHYCEAE), WITH DESCRIPTIONS OF *GONYAULAX BOHAIENSIS* SP. NOV, *G. AMOYENSIS* SP. NOV. AND *G. PORTIMONENSIS* SP. NOV.[1]

*Haifeng Gu*[2]

Department of Marine Biology and Ecology, Third Institute of Oceanography, Ministry of Natural Resources, Xiamen 361005, China

*Kenneth Neil Mertens, Amélie Derrien, Gwenael Bilien*

Ifremer, LITTORAL, Place de la Croix, BP40537, Concarneau CEDEX 29900, France

*Zhen Li*

Department of Earth, Ocean and Atmospheric Sciences, University of British Columbia, 329 West Mall, Vancouver, British Columbia V6T 1Z4, Canada

*Philipp Hess, Véronique Séchet*

Ifremer, Laboratoire Phycotoxines, Rue de l'Ile d'Yeu, Nantes 44311, France

*Bernd Krock*

Department of Ecological Chemistry, Alfred Wegener Institute for Polar and Marine Research, Am Handelshafen 12, Bremerhaven D-27570, Germany

*Ana Amorim*

Centro de Ciências do Mar e do Ambiente (MARE) and Departamento de Biologia Vegetal, Faculdade de Ciências, Universidade de Lisboa, Lisboa 1749-016, Portugal

*Zhun Li*

Biological Resource Center/Korean Collection for Type Cultures (KCTC), Korea Research Institute of Bioscience and Biotechnology, Jeongeup 56212, Korea

*Vera Pospelova*

Department of Earth and Environmental Sciences, University of Minnesota, 116 Church Street SE, Minneapolis, Minnesota 55455, USA

*Kirsty F. Smith, Lincoln MacKenzie*

Cawthron Institute, 98 Halifax Street East, Private Bag 2, Nelson 7042, New Zealand

*Joo Yeon Yoon, Hyun Jung Kim, and Hyeon Ho Shin*[2]

Library of Marine Samples, Korea Institute of Ocean Science and Technology, Geoje 53201, Korea

**The taxonomy of the extant dinoflagellate genus *Gonyaulax* is challenging since its thecate morphology is rather conservative. In contrast, cysts of *Gonyaulax* are varied in morphology and have been related with the fossil-based genera *Spiniferites* and *Impagidinium*. To better understand the systematics of *Gonyaulax* species, we performed germination experiments on cysts that can be identified as *S. ristingensis*, an unidentified *Spiniferites* with petaloid processes here described as *Spiniferites pseudodelicatus* sp. nov. and *Impagidinium variaseptum* from Chinese and Portuguese waters. Despite marked differences in cyst morphology,**

[1]Received 10 September 2021. Accepted 17 January 2022.
[2]Author for correspondence: e-mail guhaifeng@tio.org.cn (HG), shh961121@kiost.ac.kr (HS)
Editorial Responsibility: M. Cock (Associate Editor)

**motile cells of *S. pseudodelicatus* and *I. variaseptum* are indistinguishable from *Gonyaulax baltica*. Motile cells hatched from *S. ristingensis* are morphologically similar to *G. baltica* as well but differ in the presence of one pronounced antapical spine. Three new species, *Gonyaulax amoyensis* (cyst equivalent *S. pseudodelicatus*), *Gonyaulax bohaiensis* (cyst equivalent *I. variaseptum*), and *Gonyaulax portimonensis* (cyst equivalent *S. ristingensis*), were erected. In addition, a new ribotype (B) of *G. baltica* was reported from South Korea and a bloom of *G. baltica* ribotype B is reported from New Zealand. Molecular phylogeny based on LSU and SSU rRNA gene sequences revealed that *Gonyaulax* species with minute or short antapical spines formed a well-resolved clade, whereas species with two pronounced antapical spines or lack of antapical spines formed the sister clade. Six strains of four above species were examined for yessotoxin production by liquid chromatography coupled with tandem mass spectrometry, and very low concentrations of yessotoxin were detected for one *G. bohaiensis* strain.**

***Key index words:*** **Dinophyte; DNA sequencing; *Impagidinium*; LSU; *Spiniferites*; SSU; yessotoxin**

***Abbreviations*****: BI, Bayesian inference; LC–MS/MS, liquid chromatography coupled with tandem mass spectrometry; ML, maximum likelihood; PP, posterior probabilities; YTX, yessotoxin**

The fossil-based genus *Spiniferites* includes gonyaulacacean species with the Kofoidian thecal plate tabulation Po, Cp, 4′, 6″, 6c, 4–6s, 6‴, 1p, 1⁗, and they usually have trifurcate gonal and/or bifurcate intergonal processes, and a precingular archeopyle (Mertens and Carbonell-Moore 2018). To date, 106 *Spiniferites* species are accepted (Williams et al. 2017) but only 13 of them are known to be extant (Mertens and Carbonell-Moore 2018). Another fossil-based genus *Impagidinium* is morphologically similar to *Spiniferites* but lacks tri- and/or bifurcate processes (Stover and Evitt 1978). Several other fossil-based genera are morphologically similar to *Spiniferites* as well. For instance, *Achomosphaera* only differs from *Spiniferites* in the lack of sutural ridges (Evitt 1963); *Nematosphaeropsis* is distinguishable from *Spiniferites* because of the presence of trabeculae connecting the distal ends of the processes (Deflandre and Cookson 1955).

Irrespective of the morphological dissimilarity among the fossil-based genera *Spiniferites, Impagidinium,* and *Nematosphaeropsis,* all of them gave rise to motile stages attributed to the cell-based genus *Gonyaulax* (Lewis et al. 1999, Rochon et al. 2009, Mertens et al. 2018a). The first equivalencies for the genus *Spiniferites* date back to the incubation of *Spiniferites bentorii* and *S. mirabilis* from Woods Hole, MA, USA, which yielded cells identified as *Gonyaulax digitale* and *G. spinifera,* respectively (Wall and Dale 1967). Currently, eleven *Spiniferites* species have been related to *Gonyaulax* species, but several of them were attributed to *G. spinifera* (Dale 1983, Rochon et al. 2009; Table S1 in the Supporting Information), highlighting the need to examine the corresponding motile cells in detail using contemporary approaches. To date, eleven extant *Impagidinium* species have been reported (Zorzi et al. 2019). Among them, only *I. caspienense* has been related with *Gonyaulax baltica* (Mertens et al. 2018a), although *G. baltica* has been related to *Spiniferites bulloideus* sensu as well (Ellegaard et al. 2002), suggesting possible heterospory within Gonyaulacoid dinoflagellates (Mertens et al. 2018a).

*Gonyaulax* was erected to include *Gonyaulax spinifera* (Diesing 1866). The thecal plates of *Gonyaulax* are often thick and ornamented by numerous reticulations to form ridges. Its plate tabulation has been interpreted as Po, Cp, *4′, 6″, 6c, ?s, 6‴, 1p, 1⁗ (Dodge 1989, Lewis et al. 1999, Carbonell-Moore and Mertens 2019) and now includes 77 recognized species (Gómez 2012, Mertens et al. 2015, Lim et al. 2018, Gu et al. 2021). The thecate morphology of *Gonyaulax* species is rather conservative and differs between species only in the cingular displacement and overhang, the shape of the sixth precingular plate, the position of the ventral pore, the plate ornamentation, the body size, the body shape, and the number and size of antapical spines (Dodge 1989, Lim et al. 2018). Kofoid (1911) proposed to subdivide *Gonyaulax* into four subgenera (i.e., *Gonyaulax, Fusigonyaulax, Steiniella,* and *Acanthogonyaulax* based upon the general shape of the motile cells) but whether this is supported by molecular phylogenetics remains to be determined.

Several *Gonyaulax* species, identified as *Gonyaulax spinifera, G. membranacea,* and *G. taylorii* are known to produce yessotoxins (YTXs), a marine polyether toxin (Rhodes et al. 2006, Riccardi et al. 2009, Álvarez et al. 2016, Chikwililwa et al. 2019, Pitcher et al. 2019). Many strains have been identified in the literature as *G. spinifera,* but likely belong to other *Gonyaulax* species. Other *Gonyaulax* species (e.g., *G. whaseongensis*) are reported to be nontoxic (Gu et al. 2021), but the number of species examined for YTX production is still limited.

To date, only two *Impagidinium* species (*I. caspienense* and *I. pallidum*) have sequences available and *I. caspienense* groups together with *Spiniferites belerius* in molecular phylogenies, while *I. pallidum* forms a separate clade (Mertens et al. 2018a, Gu et al. 2021). To better understand the relationship between *Impagidinium* and *Spiniferites,* we isolated single cysts of *Impagidinium* and *Spiniferites* from surface sediments from Chinese, Zelanian, and Portuguese waters and performed germination experiments to obtain motile cells for SSU and LSU rRNA gene sequence analyses. Both cyst and theca morphologies were examined in detail using LM and SEM on selected strains, and molecular phylogeny was inferred based on LSU and SSU rRNA gene sequences. In addition, several *Gonyaulax* strains were established from Korean and Zelanian waters by isolating single cells and identified morphologically and by DNA sequences. Six strains of four species (two strains of both *G. bohaiensis* sp. nov. and *G. portimonensis* sp. nov., and one strain of each of *G. amoyensis* sp. nov. and *G. baltica*) were examined for YTX production by LC-MS/MS.

## MATERIALS AND METHODS

*Sample collection and treatment.* Sediment sampling was done using an Ekman grab in Qinhuangdao (Bohai Sea) and Xiamen Bay (East China Sea), China in 2018, and in Portimão, Portugal, in Oct. 2019 using a Petite Ponar Grab (Table 1). Samples were stored in the dark at 4°C until further treatment. Approximately 5 g of wet sediment was mixed with 20 mL of filtered seawater and stirred vigorously to dislodge detrital particles. The settled material was subsequently sieved through 120-μm and 10-μm mesh and washed and collected with filtered seawater. The cyst fraction was separated from this residue using sodium polytungstate at a density of 1.3 g · cm$^{-3}$ (Bolch 1997). Single cysts morphologically similar to *Impagidinium* and *Spiniferites* were isolated using a micropipette with an inverted Eclipse TS100 (Nikon, Tokyo, Japan) microscope and incubated in small containers with f/2-Si medium (Guillard and Ryther 1962) at 20°C, 90 μmol photons · m$^{-2}$ · s$^{-1}$ under a 12:12 h light:dark cycle. Fifteen Chinese culture strains of *Gonyaulax* species were established successfully (Table 1). Two Portuguese cultures were established, IFR-CC 20-019 and IFR-CC 20-018 in L1 culture medium.

Plankton samples were collected from the Korean coastal area using a 20-μm mesh plankton net. *Gonyaulax* species were isolated in laboratory using a capillary pipette with a light microscope (Eclipse 50i; Nikon, Japan) and four strains of *Gonyaulax* species (LIMS-PS-3448 (MABIK PD00002023), LIMS-PS-3408 (MABIK PD00002024), LMBE-HJ62 and LMBE-HJ86) were established successfully following the methods described by Zhang et al. (2020).

Type specimens deposited in TIO; herbarium acronyms follow (Thiers 2022).

*Morphological study of thecate stages and cysts.* Living cells and cysts of all strains or isolates listed in Table 1 were examined and photographed using a Zeiss Axio Imager light microscope (Carl Zeiss, Göttingen, Germany) equipped with a Zeiss Axiocam HRc digital camera. To observe the shape and location of the nucleus, cells were stained with 1:100,000 SYBR Green (Sigma Aldrich, St. Louis, MO, USA) for 1 min and photographed using the Zeiss fluorescence microscope with a Zeiss-filterset (excitation BP470/40, beam splitter FT495, emission BP525/50). Cell and cyst size was measured based on LM images. Portuguese and Korean strains were photographed and measured using an Olympus DP72 camera

TABLE 1. Information on *Gonyaulax bohaiensis*, *G. amoyensis*, *G. portimonensis*, and *G. baltica* isolates used in this study.

| Species | Strains | Collection date | Origin | Latitude | Longitude | Sequences | YTX fg·cell$^{-1}$ |
|---|---|---|---|---|---|---|---|
| *Gonyaulax bohaiensis* | TIO724 | June 14, 2018 | Bohai Sea | 39°56.343′ N | 119°44.738′ E | -/-/LSU | NA |
| *Gonyaulax bohaiensis* | TIO725 | June 14, 2018 | Bohai Sea | 39°56.343′ N | 119°44.738′ E | -/-/LSU | NA |
| *Gonyaulax bohaiensis* | TIO726 | June 14, 2018 | Bohai Sea | 39°56.343′ N | 119°44.738′ E | SSU/ITS/LSU | <1.34 |
| *Gonyaulax bohaiensis* | TIO727 | June 14, 2018 | Bohai Sea | 39°56.343′ N | 119°44.738′ E | -/ITS/LSU | NA |
| *Gonyaulax bohaiensis* | TIO729 | June 14, 2018 | Bohai Sea | 39°56.343′ N | 119°44.738′ E | SSU/ITS/- | NA |
| *Gonyaulax bohaiensis* | TIO730 | June 14, 2018 | Bohai Sea | 39°56.343′ N | 119°44.738′ E | -/-/LSU | NA |
| *Gonyaulax bohaiensis* | TIO731 | June 14, 2018 | Bohai Sea | 39°56.343′ N | 119°44.738′ E | -/-/LSU | NA |
| *Gonyaulax bohaiensis* | TIO732 | June 14, 2018 | Bohai Sea | 39°56.343′ N | 119°44.738′ E | SSU/ITS/LSU | 0.17 |
| *Gonyaulax bohaiensis* | LIMS-PS-3448 | Jul. 15, 2020 | Yeosu, South Korea | 34°51.569′ N | 127°43.230′ E | SSU/ITS/LSU | NA |
| *Gonyaulax amoyensis* | TIO708 | Jan. 30, 2018 | Xiamen, East China Sea | 24°35.568′ N | 118°9.198′E | SSU/ITS/LSU | NA |
| *Gonyaulax amoyensis* | TIO709 | Jan. 30, 2018 | Xiamen, East China Sea | 24°35.568′ N | 118°9.198′ E | -/ITS/LSU | NA |
| *Gonyaulax amoyensis* | TIO710 | Jan. 30, 2018 | Xiamen, East China Sea | 24°35.568′ N | 118°9.198′ E | -/ITS/LSU | NA |
| *Gonyaulax amoyensis* | TIO711 | Feb. 27, 2018 | Xiamen, East China Sea | 24°35.568′ N | 118°9.198′ E | SSU/ITS/LSU | <0.40 |
| *Gonyaulax amoyensis* | TIO713 | Feb. 27, 2018 | Xiamen, East China Sea | 24°35.568′ N | 118°9.198′ E | -/-/LSU | NA |
| *Gonyaulax amoyensis* | TIO719 | Jan. 30, 2018 | Xiamen, East China Sea | 24°35.568′ N | 118°9.198′ E | -/ITS/LSU | NA |
| *Gonyaulax amoyensis* | TIO722 | Mar. 28, 2018 | Xiamen, East China Sea | 24°35.568′ N | 118°9.198′ E | -/-/LSU | NA |
| *Gonyaulax portimonensis* | IFR20-019 | Oct. 8, 2019 | Portimão, Portugal | 37°7.202′ N | -8°31.594′ E | SSU/ITS/LSU | <0.12 |
| *Gonyaulax portimonensis* | IFR20-018 | Oct. 8, 2019 | Portimão, Portugal | 37°7.202′ N | -8°31.594′ E | SSU/ITS/LSU | <0.32 |
| *Gonyaulax baltica* | LIMS-PS-3408 | Feb. 12, 2020 | Busan, South Korea | 35°3.271′ N | 128°52.407′ E | SSU/ITS/LSU | NA |
| *Gonyaulax baltica* | LMBE-HJ62 | May 26, 2020 | Busan, South Korea | 35°3.271′ N | 128°52.407′ E | SSU/ITS/LSU | NA |
| *Gonyaulax baltica* | LMBE-HJ86 | May 25, 2020 | Busan, South Korea | 35°9.557′ N | 129°11.434′ E | SSU/ITS/LSU | NA |
| *Gonyaulax baltica* | CAWD374 | May 2019 | Māori Bay, New Zealand | 41°10.214 ′S | 173°50.218′ E | -/-/LSU | None |

Species designations, strain identification, collection date, origin, latitude, longitude, available sequences, and yessotoxin (YTX). <denotes that no concentrations were detected below this detection limit. NA: not available.

mounted on a BX41 microscope with 1009 oil immersion objectives and a Nikon DS-Ri2 camera mounted on a ECLIPSE Nikon microscope, respectively.

For SEM, mid-exponential batch cultures of selected Chinese strains were concentrated by a Universal 320 R centrifuge (Hettich-Zentrifugen, Tuttlingen, Germany) following standard protocols (Gu et al. 2021) and examined with a Zeiss Sigma FE (Carl Zeiss, Oberkochen, Germany) SEM at Xiamen University, China.

For SEM observations of Portuguese strains, cells were picked from microwells using a IX70 (Olympus) inverted microscope and filtered using polycarbonate membrane filters (0.22 μm pore size, GTTP Isopore, Millipore, Billerica, MA, USA), and filters were processed according to the methods described in Chomérat and Couté (2008). They were dehydrated in a graded series of ethanol baths (15–100%), critical-point-dried, sputter coated with gold. Cells on the stubs were examined at the Station of Marine Biology in Concarneau using a Sigma 300 Gemini (Zeiss, Obserkochen, Germany) field-emission SEM equipped with both a conventional Everhart-Thornley and in-lens secondary electron detectors, operated at 5 kV.

For SEM observations of Korean strains, 2 mL of mid-exponential batch cultures of strains were fixed by Lugol's Iodine solution (0.1% final concentration) for 24 h at room temperature and then rinsed by centrifugation with deionized water. After rinsing, samples were dehydrated, critical point dried, and examined following standard protocols (Zhang et al. 2020). Tabulation labeling follows the Kofoid system (Kofoid 1911). The sulcal plate labeling follows Balech (1980).

*PCR amplifications and sequencing.* Single cells of Chinese strains were isolated and washed several times with sterile distilled water. They were broken by applying gentle force on the coverslip with the inverted microscope and pipetted into a PCR tube for templates. Various regions of rRNA genes including the SSU, partial LSU (D1–D6) and ITS1–5.8S–ITS2 were amplified using primer pairs specified previously and following standard protocols (Luo et al. 2019).

For Korean strains, genomic DNA was extracted from 1 mL of exponentially growing cultures using the DNeasy Plant Mini Kit (QIAGEN Inc., Valencia, CA, USA) following the manufacturer's instructions. The SSU, ITS1-5.8S-ITS2, and LSU rDNA sequence were amplified using the primer pairs SR1 and SR12b, SSUITS and 25R1, and 25F1, and R2 (Yamaguchi and Horiguchi 2005, Takano and Horiguchi 2006) following standard protocols (Zhang et al. 2020).

For Portuguese strains, genomic DNA was extracted from 20 μL of exponentially growing cultures using the PCRBIO Rapid extract PCR kit (PCR Biosystems Ltd, London, UK) following the manufacturer's instructions. Almost the full length of the SSU rDNA was specifically amplified using primers 18S-FW and 18S-RV and for the ITS1-5.8S-ITS2-LSU rDNA, an amplicon of more than 1300 bp was obtained with primers ITS-Fw and D3B (Nézan et al. 2012) following standard protocols (Gu et al. 2021). For the New Zealand strain, genomic DNA extraction, PCR and sequencing conditions for the LSU rRNA were performed as described in Smith et al. (2016). Newly obtained sequences were deposited in GenBank with accession numbers OM177644 to OM177653 and OM228714 to OM228731.

*Sequence alignment and phylogenetic analysis.* Newly obtained LSU rRNA (ca. 1,300 bp) and SSU rRNA (ca. 1,700 bp) gene sequences were aligned with sequences of *Gonyaulax* species and related taxa available in GenBank. Sequences were aligned using MAFFT v7.110 (Katoh and Standley 2013) online program (http://mafft.cbrc.jp/alignment/server/) with default settings. Alignments were manually checked with BioEdit v7.0.5 (Hall 1999). The final alignment consisted of 1527 LSU rRNA and 1841 SSU rRNA base pairs including introduced gaps. For Bayesian inference (BI), the program jModelTest (Posada 2008) was used to select the most appropriate model of molecular evolution with Akaike information criterion (AIC). Bayesian reconstruction of the data matrix was performed using MrBayes 3.2 (Ronquist and Huelsenbeck 2003) with the best-fitting substitution model (GTR+G). Four Markov chain Monte Carlo (MCMC) chains ran for 2,000,000 generations, sampling every 1,000 generations. The first 10% of burn-in trees were discarded. A majority rule consensus tree was created to examine the posterior probabilities (PP) of each clade. Maximum likelihood (ML) analyses were conducted with RaxML v7.2.6 (Stamatakis et al. 2008) on the T-REX web server (Boc et al. 2012) using the model GTR+G. Bootstrap support (BS) was assessed with 1000 replicates.

*Yessotoxin analysis.* Cultures of six strains (TIO726, TIO732, TIO711, IFR20-018, IFR20-019, and CAWD374) were grown in 200 mL Erlenmeyer flasks under standard culture conditions. At the stationary phase (determined using sequential cell counts), ~$10^5$–$10^6$ cells were concentrated by a Universal 320 R centrifuge (Hettich-Zentrifugen, Tuttlingen, Germany) at 2500*g* for 10 min at 4 °C. Cell pellets for quantification of intracellular YTX were transferred to 2 mL microcentrifuge tubes and stored at −20°C until analysis. Measurements were carried out by liquid chromatography (LC 1100. Agilent, Waldbronn Germany) coupled to tandem mass spectrometry (API 4000 QTrap, Sciex, Darmstadt Germany) as detailed in Wang et al. (2019). Yessotoxins were screened in the negative mode by selected reaction monitoring (SRM). Screened YTX variants and their respective mass transitions are given in supplemental materials (Table S2 in the Supporting Information).

For strains TIO732, IFR20-019, and IFR20-018, sample analyses were performed by LC–MS/MS using a Shimadzu UFLCxr system coupled to a triple quadruple hybrid mass spectrometer Q-Trap (API400QTrap, Sciex) equipped with a heated electrospray ionization (ESI) source. Data acquisitions were performed in negative ion mode and using MRM (Multiple Reaction Monitoring) mode. Chromatographic separation was carried out on a reversed-phase column Xbridge BEH C18 (50 × 2.1 mm, 2.5 μm, Waters) equipped with a guard column (5 × 2.1 mm, 2.5 μm, same stationary phase as column). Water (A) and acetonitrile 90% (B) both containing 6.7 mM of ammonium hydroxide were used as mobile phases at a flow rate of 400 $\mu L \cdot min^{-1}$. The following gradient was used: 0 min, 5% B; 1.5 min, 5% B; 4.5 min, 65% B; 5.0 min, 100% B; 7.0 min, 100% B; 7.5 min, 5% B; 12.0 min, 5% B. The oven temperature was 30°C and the injection volume was 5 μL. The LC–MS/MS method was used to detect 13 toxins (Table S3 in the Supporting Information). Quantification was performed relative to YTX and homo-YTX standards (National Research Council Canada) with a 6-point calibration curve. The limit of quantification was 0.03 $ng \cdot mL^{-1}$ for YTX and homo YTX standards. The ESI interface was operated using the parameters described in Wang et al. (2019).

## RESULTS

In this study, 22 strains of *Gonyaulax* were established and identified based on the morphology of both cysts and thecae and confirmed by DNA sequences. Nine strains were identified as *G. bohaiensis* sp. nov (cyst equivalent *Impagidinium variaseptum*), seven strains as *G. amoyensis* sp. nov. (cyst equivalent *Spiniferites pseudodelicatus*), two strains as *G. portimonensis* sp. nov. (cyst equivalent *S. ristingensis*), and four strains as *G. baltica* (Table 1).

*Gonyaulax baltica* from the Pacific proved to be genetically separated from those in the Atlantic and formed a new ribotype. Only one strain of *G. bohaiensis* tested positive for YTX production.

Gonyaulax bohaiensis *H. Gu, K.N. Mertens & H.H. Shin sp. nov. Description*: Cells were 25–46 μm long and 21–37 μm wide with numerous minute antapical spines (Figs. 1, 2, Figs. S1-S3 in the Supporting Information). The epitheca was conical with intermediate shoulders. The cell surface was thick and reticulated. Small pores were scattered over the thecal plates and were aligned along the cingulum. The sulcal plates bore neither pores nor reticulation. The torsion was neutral. The cingulum was located in the equatorial part of the cell and descended with a displacement and overhang of about 2.5 times its width. Sexiform hypothecal configuration. Cells displayed a plate formula of Po, Cp, 4′, 6″, 6C, 6S, 5‴, 1p, 1⁗. Plate 6″ was very elongated. A ventral pore was located at the junction of plates 1′, 4′a, and 4′p. The angle between the major axis and a line joining the ends of the cingulum was approximately 35–45°. The cyst was subspherical to ellipsoidal, 36–41 μm long and 30–36 μm wide with an apical boss (excluding the crests). The cyst had low sutural septa 2.0–4.8 μm high, except around the antapical plate where the septa were 4.0–7.6 μm high. The cyst displayed a paratabulation of 4′, 6″, 6C, 6S, 5‴, 1p, 1⁗. The paracingulum descended with a displacement of two-three times its width. The archeopyle was reduced and corresponded to plate 3″.

*Holotype* (designated here): TIO 202201, SEM stub of thecate cells from a culture established from a cyst extracted from surface sediment of Bohai Sea, June 14, 2018, collected by Haifeng Gu.

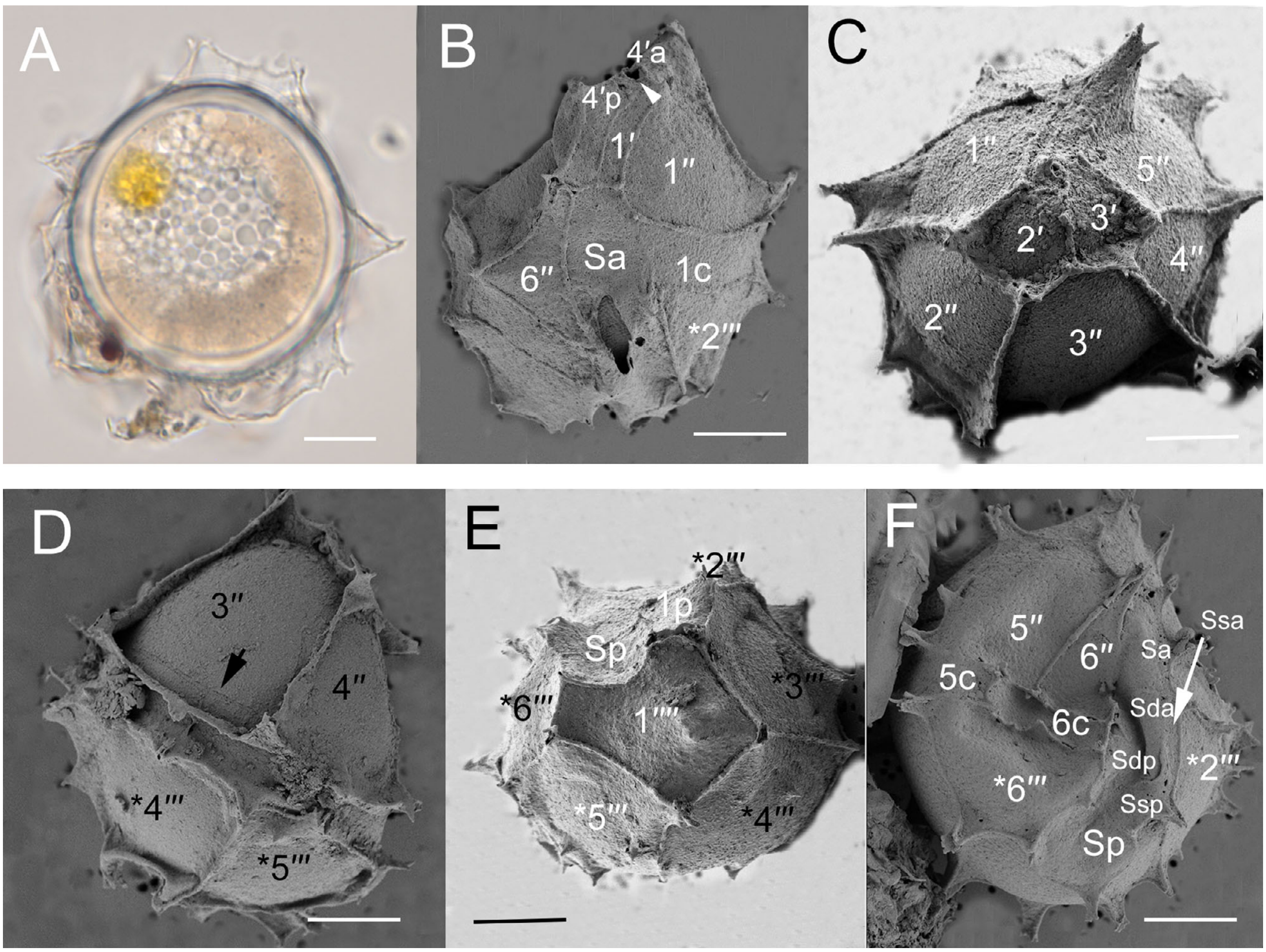


FIG. 1. Micrographs of cysts of *Gonyaulax bohaiensis* from the Bohai Sea, China, resembling *Impagidinium variaseptum*. Tabulation labeling follows Kofoid (1911) and Balech (1980). (A) Bright-field light microscopy. (B–F) Scanning electron microscopy. (A) A living cyst showing the yellow accumulation body and sutural septa of variable height. (B) Ventral view of a living cyst showing a ventral pore (arrow). (C) Apical view of a living cyst showing two apical (2′, 3′) and five precingular plates (1″–5″). (D) Dorsal view of an empty cyst showing the reduced archeopyle (arrow). (E) Antapical view showing five postcingular (*2‴–*6‴) plates, one antapical plate (1⁗) and one intercalary plate (1p) (F) Ventral view of a living cyst showing the anterior sulcal plate (Sa), anterior left sulcal (Ssa) plate, posterior left sulcal (Ssp), right anterior sulcal plate (Sda), right posterior sulcal plate (Sdp), and posterior sulcal plates (Sp). Scale bars = 10 μm. [Color figure can be viewed at wileyonlinelibrary.com]

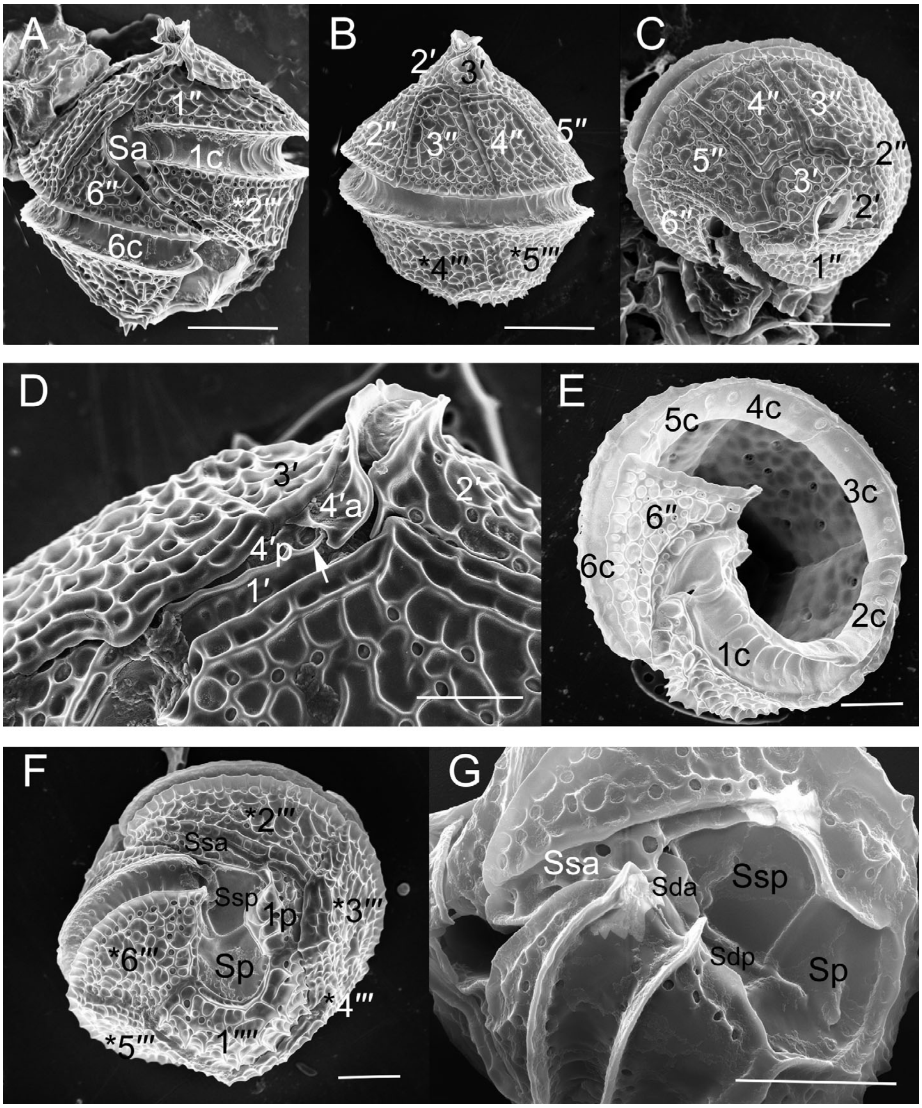


FIG. 2. Scanning electron micrographs of *Gonyaulax bohaiensis* strain TIO726 from the Bohai Sea, China. (A) Ventral view showing cingulum displacement and overhang. (B) Dorsal view showing four precingular (2″–5″), and two postcingular (*4‴, *5‴) plates. (C) Apical view showing six precingular (1″–6″), and two apical (2′, 3′) plates. (D) Apical–ventral view showing the first and fourth apical plates (1′, 4′) and a ventral pore (arrow). (E) The cingulum showing six cingular plates. (F) Antapical view showing five postcingular (*2‴–*6‴) plates, one antapical plate (1⁗), and one intercalary plate (1p). (G) Sulcal plates showing the anterior left sulcal plate (Ssa), anterior right sulcal plate (Sda), posterior left sulcal plate (Ssp), posterior right sulcal plate (Sdp), and posterior sulcal plate (Sp). Scale bars = 4 μm, except in (A–C) = 10 μm.

*Type locality*. Bohai Sea; 39°56.34′ N, 119°44.74′ E.

*Habitat*. Marine and planktonic with benthic cyst stage.

*Etymology*. The epithet "*bohaiensis*" is derived from Bohai Sea and refers to the type locality.

*GenBank accession numbers*. OM177646 (SSU rRNA gene), OM228722 (LSU rRNA gene).

*Remarks*. The morphology of the cyst resembles the fossil-based taxon *Impagidinium variaseptum* (see discussion).

*Morphology*. Cysts of *Gonyaulax bohaiensis* had a subspherical to ellipsoidal central body with one pronounced yellow-orange accumulation body, many transparent lipid bodies and a spherical nucleus (Figs. 1A, S1A). They were 36.0–40.5 μm in length (mean = 37.9 ± 1.4 μm, $n$ = 8) and 30.0–36.0 μm in width (mean = 33.5 ± 1.9 μm, $n$ = 8). The central body wall was formed of pedium and tegillum. The pedium was smooth, and the tegillum was microgranulate and formed the parasutural crests. The height of the parasutural septa was 2.0–4.8 μm (mean = 3.5 ± 1.1 μm, $n$ = 8), except around the antapical paraplate where the septa were higher (4.0–7.6 μm, mean = 5.9 ± 1.2 μm, $n$ = 6; Fig. 1, A and C). The septa could form short, exclusively gonal processes which can have minute furcations. The epicyst had a smooth rounded apex with an apical boss (Fig. 1, B, C and F). There was a ventral pore at the junction of plates 1′, 4′a, and 4′p (Fig. 1B). The parasutures between 1′ and 4′ were faintly visible. Plate 6″ was very elongated. The paracingulum descended with a displacement of two to three cingular widths (Fig. 1, B and F). The parasulcal plates were sometimes faintly discernable. The torsion was neutral (Fig. 1D). The archeopyle was precingular and reduced corresponding to paraplate 3″ (Fig. 1D). The operculum was monoplacate and free (Fig. S1B). Cysts of *G. bohaiensis* were commonly found in Bohai Sea.

Cells of *Gonyaulax bohaiensis* strain TIO726 were 25.3–45.6 μm (mean = 31.3 ± 3.7 μm, $n$ = 52) long and 21.1–37.0 μm (mean = 26.0 ± 3.4 μm, $n$ = 52) wide. Cells had a conical epitheca with intermediate shoulders and a rounded hypotheca (Fig. 2, A and B). There were numerous bean-shaped chloroplasts located in the periphery of the cell (Fig. S1, C and D). The nucleus was elongated and curved, extending from the left epicone to the right hypocone (Fig. S1, D and E).

The thecae had a sexiform gonyaulacoid tabulation in the hypotheca (sensu Fensome et al. 1993, their text-fig. 64B) with a S-type ventral organization (sensu Fensome et al. 1993, text- fig. 82, B and D) and neutral torsion (sensu Fensome et al. 1993, text-fig. 83B; Fig. 2, A–D).

The pore plate was lanceolate in shape and surrounded by raised ridges of neighboring apical plates (Fig. 2D). The first and fourth apical plates (1′, 4′) were small and narrow (Fig. 2, B and C). A ventral pore was observed at the junction of plates 1′, 4′a (anterior part of 4′), and 4′p (posterior part of 4′; Figs. 2D, S1F). The plate 6″ was triangular (Fig. 2A). The cingulum descended with a displacement of around 2.5 widths (Fig. 2A) and an overhang also around 2.5 widths (Fig. 2E).

All postcingular plates were similar in size. Plate 1p was located adjacent to plates Sp and Ssp (Fig. 2F). Plate 1⁗ was located in the middle of the hypotheca with numerous short spines approximately 1.0 μm long (Fig. 2F). The sulcus was narrow in the middle but wide at both ends. It was comprised of the anterior sulcal plate (Sa), the anterior left sulcal (Ssa) plate, the posterior left sulcal (Ssp), the right anterior sulcal plate (Sda) and right posterior sulcal plate (Sdp) and posterior sulcal plates (Sp; Fig. 2, F and G). A schematic plate pattern is provided in Fig. S2. Cells of the Korean strain LIMS-PS-3448 were morphologically similar to the Chinese strains, but differed in possessing several medium-sized antapical spines (Fig. S3, A–E). Plates 3″ and *4‴ were identified as the keystone plates (Fig. S3, D and E).

Gonyaulax amoyensis *H. Gu & K.N. Mertens sp. nov. Description.* Cells were 24–42 μm long and 19–29 μm wide with numerous minute antapical spines (Figs. 3, 4, Figs. S4 and S5 in the Supporting Information). The epitheca was conical with short shoulders. The cell surface was thick and reticulated. The cingulum was located in the equatorial part of the cell and descended with a displacement and overhang of around 2.5 widths. Cells displayed a plate formula of Po, Cp, 4′, 6″, 6C, 6S, 5‴, 1p, 1⁗. A ventral pore was present at the junction of plates 1′, 4′a, and 4′p. The angle between the major axis and a line joining the ends of the cingulum was approximately 25–35°. The cyst was ovoid to ellipsoidal, 29–40 μm long and 26–36 μm wide with a low apical boss. They were ornamented with gonal (occasional intergonal), petaloid processes 6–13 μm long, and connected by low-to-high membranous flanges. The paracingulum descended with a displacement of two to three times its width. The archeopyle was reduced and corresponded to plate 3″.

*Holotype* (designated here). TIO 202202, SEM stub of thecate cells from a culture established from a cyst extracted from surface sediment of East China Sea on February 27, 2018, collected by Haifeng Gu.

*Type locality.* East China Sea; 24°35.57′ N, 118°9.20′ E.

*Habitat.* Marine and planktonic with benthic cyst stage.

*Etymology.* The epithet "*amoyensis*" is derived from Amoy, the old English name based on the Hokkien pronunciation of Xiamen, and refers to the type locality.

*GenBank accession numbers.* OM177649 (SSU rRNA gene), OM228717 (LSU rRNA gene).

*Remarks.* The geological preservability of these cysts was demonstrated by their ability to withstand palynological treatment. The cyst resembles the fossil-based taxon *Spiniferites pseudodelicatus* described below.

Spiniferites pseudodelicatus *K.N. Mertens & H. Gu sp. nov. Description.* The cyst was subspherical to ellipsoidal, 36–41 μm long and 30–36 μm wide with an apical boss (excluding the crests; Fig. 3C). The cyst had sutural septa 2–5 μm high, except around the antapical plate where the septa were 4–8 μm high. The cyst had a tabulation of 4′, 6″, 6C, 6S, 5‴, 1p, 1⁗. The paracingulum descended with a displacement of two-three times its width. The archeopyle was reduced and corresponded to plate 3″.

*Holotype* (designated here): FR CEDiT2022H137, SEM stub from a cyst isolated from surface sediment collected on May 26, 2008, by Dong Xu. Dinoflagellate type collection in the Centre of Excellence for Dinophyte Taxonomy (CEDiT, Wilhelmshaven, Germany).

*Type locality.* South China Sea (21°19.80′ N,111°10.20′ E, 17.5 m water depth).

*Habitat.* Marine.

*Etymology.* The epithet "*pseudodelicatus*" was chosen because of the superficial morphological similarity of the cyst to *Spiniferites delicatus.*

*Morphology.* Cysts of *Gonyaulax amoyensis* had an ovoid to ellipsoidal central body and were 28.7–39.6 μm (mean = 32.2 ± 3.9 μm, $n$ = 6) long and 26.2–35.6 μm (mean = 29.9 ± 3.1 μm, $n$ = 6) wide.

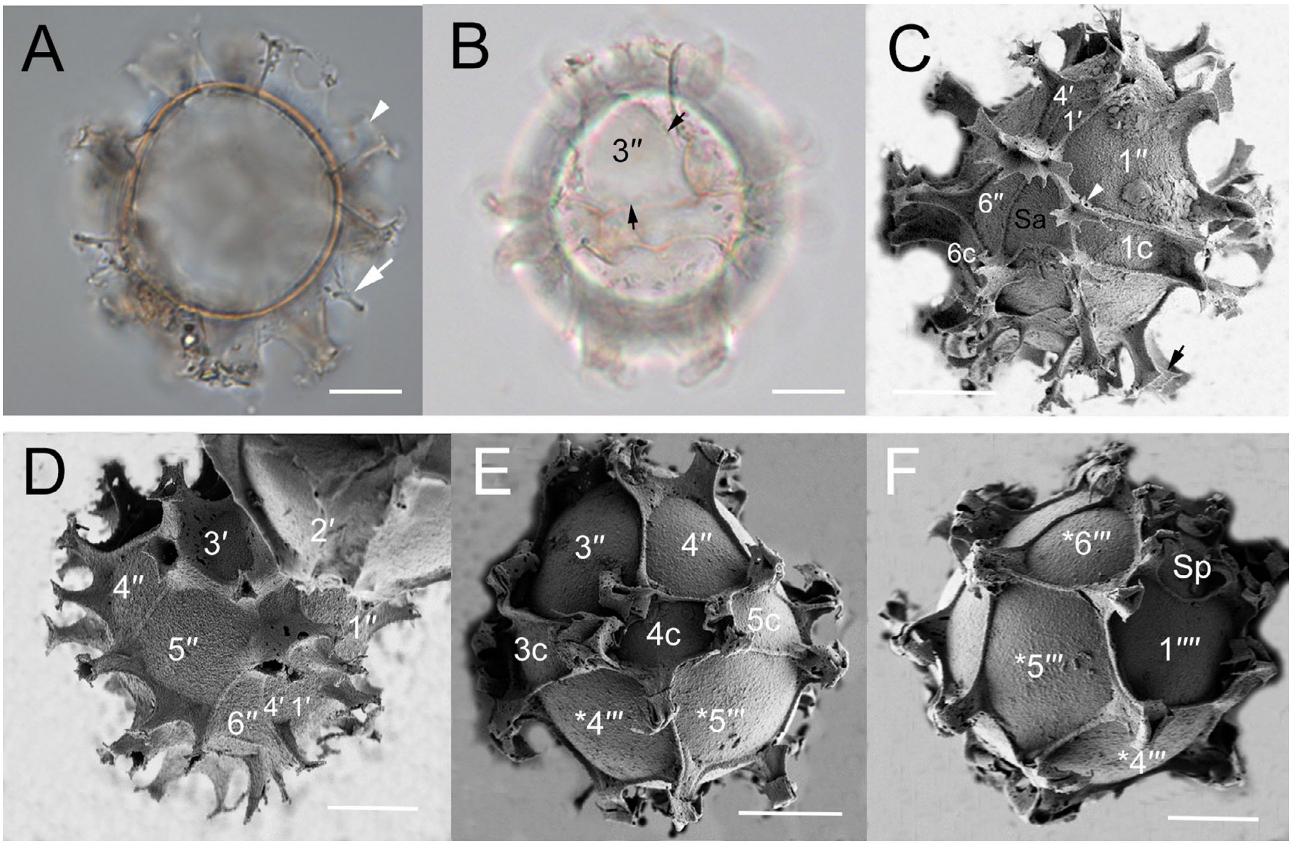


FIG. 3. Micrographs of *Gonyaulax amoyensis* cysts from Xiamen Bay, China (A, B, D), and *Spiniferites pseudodelicatus* from the South China Sea (C, E, F). (A, B) Bright-field light microscopy. (C–F) Scanning electron microscopy. (A) An empty cyst showing the undeveloped intergonal process (arrow) and membrane connecting gonal processes (arrowhead). (B) Dorsal view of an empty cyst showing the reduced archeopyle (arrows). (C) Ventral view of an empty cyst showing the cingulum displacement, claustra (arrowhead) and petaloid processes (arrow). (D) Apical view of a living cyst showing the apical plates. (E) Dorsal view of a living cyst. (F) Antapical view of a living cyst. Scale bars = 10 μm. [Color figure can be viewed at wileyonlinelibrary.com]

The central body wall was formed of pedium and tegillum. The pedium was smooth, and the tegillum was microgranulate and formed the parasutural crests. They were ornamented with processes 5.6–12.9 μm long (mean = 7.9 ± 1.9, $n$ = 21) and connected by low to mid-high membranous flanges (Fig. 3A). The paracingulum descended with two-three times of its widths (Figs. 3C, S4A). The cyst wall was 0.8–1.2 μm thick (mean = 1.1 ± 0.2 μm, $n$ = 5). The processes were gonal, wide, petaloid and trumpet-shaped with multifurcated tips (Fig. 3, C and D). Occasionally, an intergonal process was observed in the postcingular paraseries, which did not show furcated tips (Fig. 3A). A low apical boss was observed (Fig. 3C). The archeopyle was reduced, corresponding to plate 3″ (Fig. 3E). The operculum was monoplacate and free (Fig. 3B). Claustra (large arched openings) could be observed at the base of the parasutures (Fig. 3C).

Cells of *Gonyaulax amoyensis* strain TIO711 were 23.8–42.4 μm long (mean = 32.6 ± 3.7 μm, $n$ = 28) and 19.2–29.1 μm wide (mean = 25.2 ± 2.8 μm, $n$ = 28). Cells had a conical epitheca with intermediate shoulders and a rounded hypotheca (Fig. S4, A and B). There were numerous bean-shaped chloroplasts located in the periphery of the cell (Fig. S4, A and B). The nucleus was elongated and located in the hypocone (Fig. S4, C and D).

Thecae had a sexiform gonyaulacoid tabulation in the hypotheca with an S-type ventral organization and neutral torsion (Fig. 4, A and C). The pore plate was lanceolate in shape and surrounded by raised ridges of neighboring apical plates (Fig. 4A). Plates 1′ and 4′ were very narrow (Fig. 4, D and F). The cingulum was situated in the equatorial part of the cell, descending with a displacement of 2-3 cingulum widths (Fig. 4, A and B). The cingulum overhang was 1.8–2.5 widths (Fig. 4G).

Plate 1⁗ had numerous short spines ca. 0.6 μm long (Fig. 4H). The sulcus was wide in the anterior and posterior part but narrow in the central part. It was comprised of plates Sa, Ssa, Ssp, Sda, Sdp, and Sp (Fig. 4, A and I). A schematic plate pattern is provided in Figure S5. Plates 3″ and *4‴ were identified as the keystone plates (Fig. 4C).

Gonyaulax portimonensis *sp. nov. K.N. Mertens, A. Amorim & H. Gu sp. nov.* *Description.* Cells were 30–43 μm long and 24–39 μm wide with 2–4 short

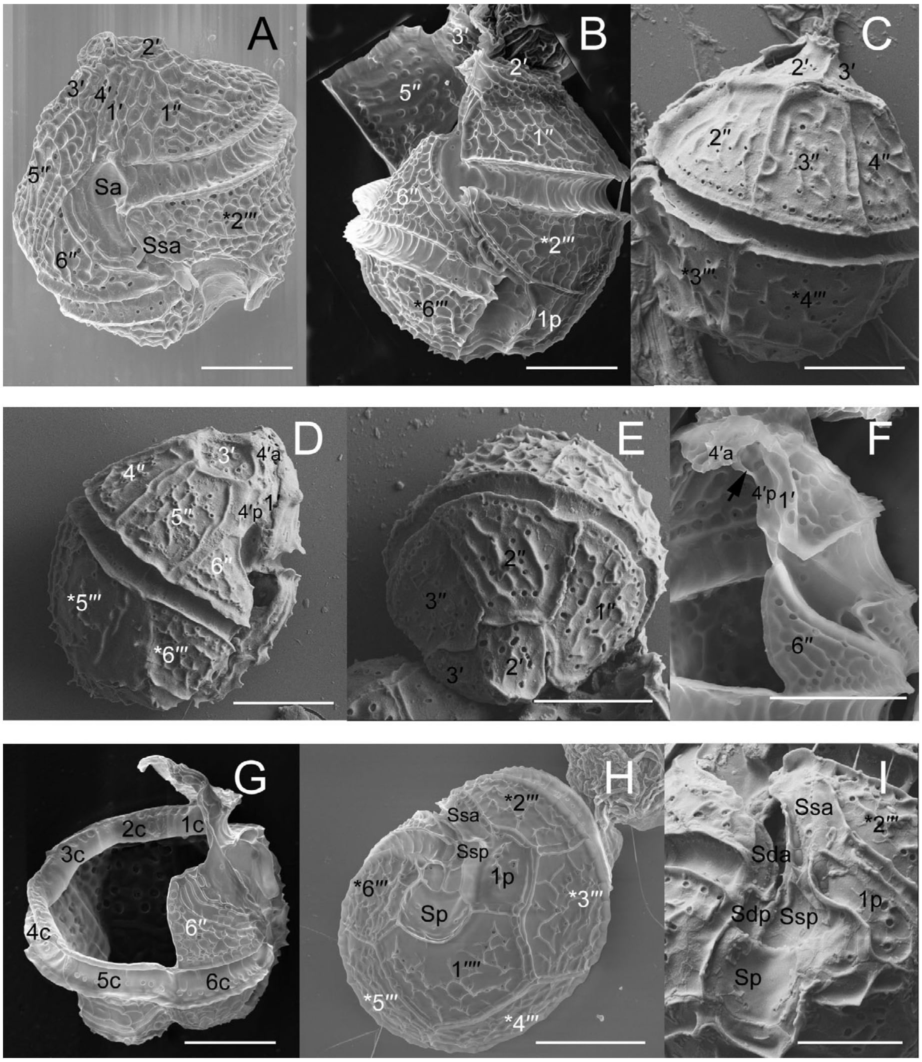


FIG. 4. Scanning electron micrographs of *Gonyaulax amoyensis* strain TIO711 from Xiamen Bay, China. (A, B) Ventral view showing cingulum displacement and overhang. (C) Dorsal view showing three precingular (2″–4″), and two postcingular (*3‴, *4‴) plates. (D) Lateral view showing three precingular (4″–6″), three apical plates (1′, 3′, 4′). (E) Apical view showing three precingular (1″–3″), and two apical (2′, 3′) plates. (F) Ventral view showing the two apical (1′, 4′) plates and a ventral pore (arrow). (G) The cingulum showing six cingular plates. (H) Antapical view showing five postcingular (*2‴–*6‴) plates, one antapical plate (1⁗) and one intercalary plate (1p). (I) Sulcal plates showing the anterior left sulcal plate (Ssa), anterior right sulcal plate (Sda), posterior left sulcal plate (Ssp), posterior right sulcal plate (Sdp), and posterior sulcal plate (Sp). Scale bars = 10 μm.

antapical spines, often with a pronounced right antapical horn (Figs. 5, 6, Fig. S6 in the Supporting Information). Epitheca was conical with short shoulders. Cell surface was thick and formed dense reticulations. Cingulum was located in the equatorial part of the cell and descended with a displacement and overhang of about 2.0 times its width. Cells displayed a plate formula of Po, Cp, 4′, 6″, 6C, 6S, 5‴, 1p, 1⁗. Angle between the major axis and line joining ends of cingulum was approximately 25–40°. Cyst was subspherical to ellipsoidal, 42–48 μm long and 32–38 μm wide with apical boss. Cyst had gonal, petaloid processes, 12–14 μm in length, connected by low sutural crests. Cyst wall was formed of a smooth pedium and a tegillum that formed small blisters and hollow undulations over the surface. Paracingulum descended with displacement of three times its width. Archeopyle was not reduced and corresponded to plate 3″.

*Holotype* (designated here): FR CEDiT2022H136, SEM stub containing the type specimen from a culture established from a cyst isolated from surface sediment collected on October 8, 2019, by Véronique Séchet and K.N. Mertens. Dinoflagellate type collection in the Centre of Excellence for Dinophyte Taxonomy (CEDiT, Wilhelmshaven, Germany).

*Type locality*. Portimão Port, Portugal (37°7.20′ N, −8°31.59′ E).

*Habitat*. Marine and planktonic with benthic cyst stage.

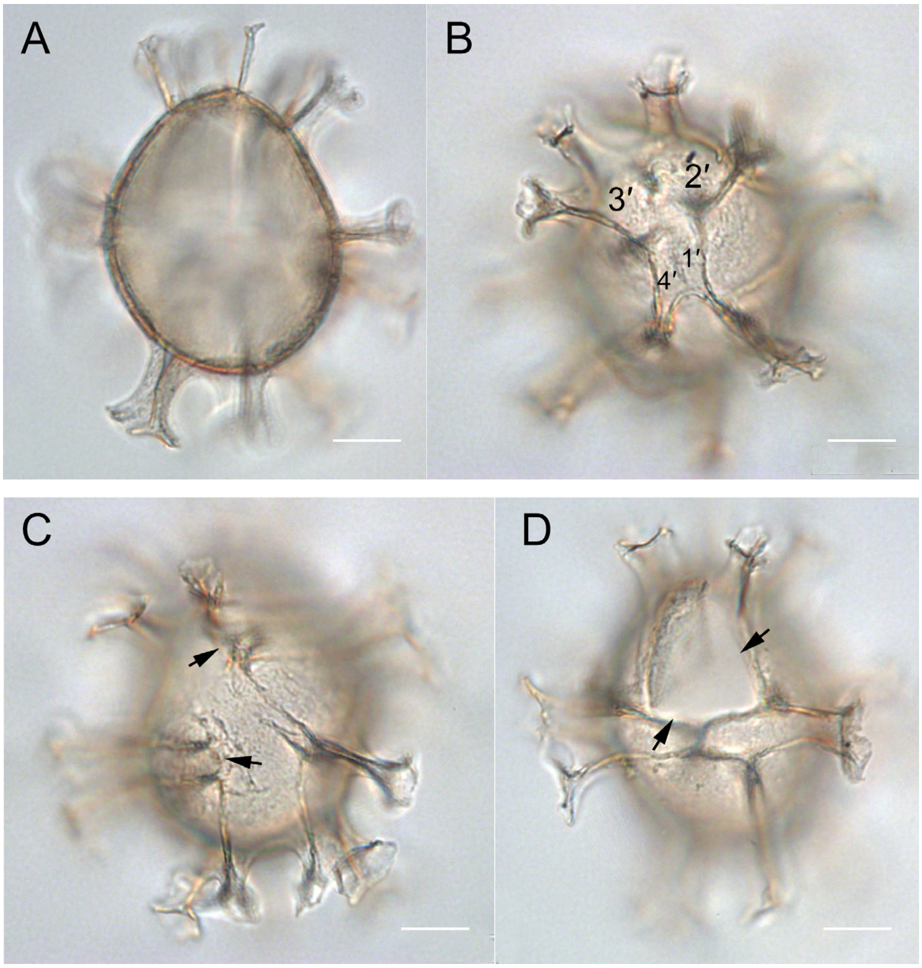


FIG. 5. Light micrographs of cysts resembling *Spiniferites ristingensis* from Portugal. (A) An empty cyst showing the ovoid body and a low apical boss. (B) Apical–ventral view of an empty cyst showing the apical plates. (C) Ventral view of an empty cyst showing the cingulum displacement (arrows). (D) Dorsal view of an empty cyst showing the archeopyle not reduced (arrows). Scale bars = 10 μm. [Color figure can be viewed at wileyonlinelibrary.com]

*Etymology*. The epithet "*portimonensis*" is derived from Portimão and refers to the type locality.

*GenBank accession numbers*. OM177644 (SSU rRNA gene), OM228730 (LSU rRNA gene).

*Remarks*. The cyst resembles the fossil-based taxon *Spiniferites ristingensis* (see discussion).

*Morphology*. Cysts of *Gonyaulax portimonensis* were ovoid, 41.7–47.7 μm (mean = 45.0 ± 3.0 μm, $n$ = 3) long and 31.9–38.3 μm (mean = 36.0 ± 3.6 μm, $n$ = 3) wide (Fig. 5A). They were ornamented with processes 11.5–14.0 μm in length (mean = 12.9 ± 1.0, $n$ = 9) and connected by low sutural crests, but sometimes by high membranous flanges (Fig. 5B). The cingulum descended with three times of its width (Fig. 5C). The cyst wall, ca 1.3 μm thick, was formed of a smooth pedium and a tegillum that formed small blisters and hollow undulations over the surface, that appeared granulate (Fig. 5B). The processes were gonal, petaloid, forming polygonal platforms (Fig. 5C). A low apical boss was observed (Fig. 5A). Parasulcal plates were expressed. The archeopyle was not reduced, corresponding to plate 3″ (Fig. 5D). The operculum was monoplacate and free.

Cells of *Gonyaulax portimonensis* strain IFR20-019 were 30.0–42.9 μm long (mean = 34.8 ± 3.7 μm, $n$ = 17) and 24.4–38.6 μm wide (mean = 30.6 ± 3.6 μm, $n$ = 17). Cells had a conical epitheca with intermediate shoulders and a rounded hypotheca (Fig. S6A). There were numerous bean-shaped chloroplasts located in the periphery of the cell (Fig. S6, B and C). The nucleus was large and located in the hypocone (Fig. S6C).

The thecae had a sexiform gonyaulacoid tabulation (Fig. 6E) with an S-type ventral organization and neutral torsion (Fig. 6, A and B). The pore plate was lanceolate in shape and surrounded by raised ridges of neighboring apical plates (Fig. 6, C and D). There was a ventral pore between plates 4′a and 4′p (Figs. 6D, S6D). The cingulum descended with a displacement of two cingulum widths (Figs. 6A, S6A). The cingulum overhang was ca. two

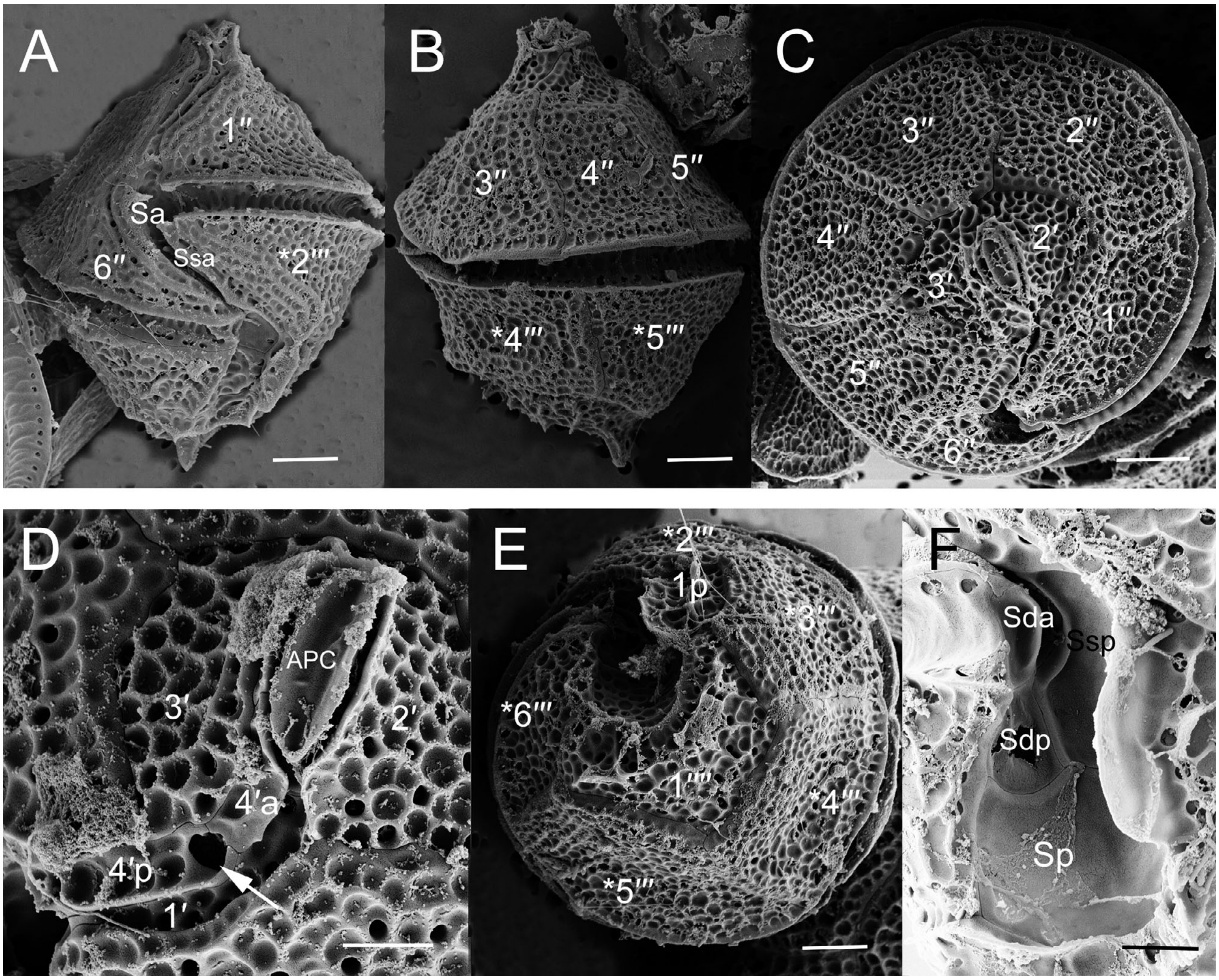


Fig. 6. Scanning electron micrographs of *Gonyaulax portimonensis* from Portugal. (A) Ventral view showing cingulum displacement and overhang and a pronounced antapical spine. (B) Dorsal view showing three precingular (3″–5″) and two postcingular (*4‴, *5‴) plates. (C) Apical view showing six precingular (1″–6″), and two apical (2′, 3′) plates. (D) Apical view showing the four apical (1′–4′) plates, APC and a ventral pore (arrow). (E) Antapical view showing five postcingular (*2‴–*6‴) plates, one antapical plate (1⁗) and one intercalary plate (1p). (F) Sulcal plates showing the anterior left sulcal plate (Ssa), anterior right sulcal plate (Sda), posterior left sulcal plate (Ssp), posterior right sulcal plate (Sdp) and posterior sulcal plate (Sp). Scale bars = 5 μm, except in (D) = 2 μm.

widths. Plate 1⁗ had 2–4 short spines 1.5–4.3 μm long (Fig. 6, B and E). The sulcus was narrow in the middle but wide in the anterior and posterior parts. It was comprised of plates Sa, Ssa, Ssp, Sda, Sdp, and Sp (Fig. 6F). A schematic plate pattern is provided in Figure S7 in the Supporting Information. Plates 3″ and *4‴ were identified as the keystone plates (Fig. 6, B and E).

Gonyaulax baltica. *Morphology.* Cells of Korean strain LIMS-PS-3408 were 27.6–44.5 μm long (mean = 35.1 ± 4.2 μm, *n* = 30) and 23.0–34.9 μm wide (mean = 28.7 ± 2.6 μm, *n* = 30). Cells had a conical epitheca with intermediate shoulders and a rounded hypotheca (Fig. S8A in the Supporting Information). There were numerous bean-shaped chloroplasts located in the periphery of the cell (Fig. S8B). The nucleus was variable ranging from L-shaped to short curved, located in the hypocone (Fig. S8, D–F).

Cells had a plate formula of Po, Cp, 4′, 6″, 6C, 6S, 5‴, 1p, 1⁗ (Fig. 7). The thecae had a sexiform gonyaulacoid hypotheca tabulation with a S-type ventral organization and neutral torsion (Fig. 7, A and B). The pore plate was lanceolate in shape and surrounded by raised ridges of neighboring apical plates (Fig. 7C). There was a ventral pore between plates 4′a and 4′p (Fig. 7C). The cingulum descended with a displacement of three cingulum widths (Fig. 7A). The cingulum overhang was ca. 2.5 widths. The angle between the major axis and a line joining the ends of the cingulum was approximately 40–45°. Plate 1⁗ had numerous short spines ca. 0.6 μm long (Fig. 7, A and E). The sulcus was narrow in the middle but widened toward anterior

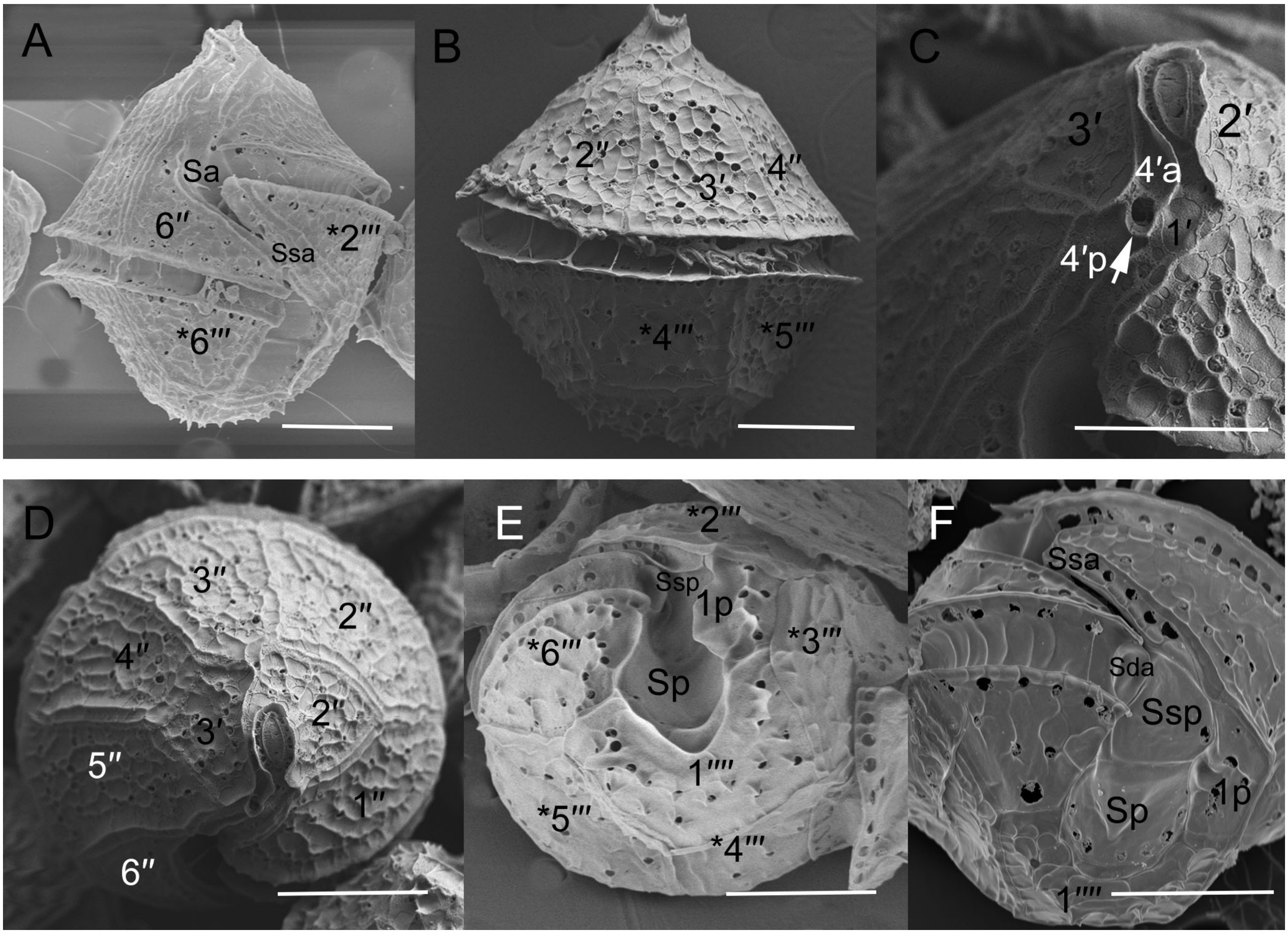


FIG. 7. Scanning electron micrographs of *Gonyaulax baltica* strain LIMS-PS-3408 from South Korea. (A) Ventral view showing cingulum displacement and overhang. (B) Dorsal view showing three precingular (2″–4″), and two postcingular (*4‴, *5‴) plates. (C) Apical view showing two apical (1′, 4′) plates, and a ventral pore (arrow). (D) Apical view showing six precingular (1″–6″), and two apical (2′, 3′) plates. (E) Antapical view showing five postcingular (*2‴–*6‴) plates, one antapical plate (1⁗) and one intercalary plate (1p). (F) Sulcal plates showing the anterior left sulcal plate (Ssa), anterior right sulcal plate (Sda), posterior left sulcal plate (Ssp), and posterior sulcal plate (Sp). Scale bars = 10 μm.

and posterior parts. It comprised of plates Sa, Ssa, Ssp, Sda, Sdp, and Sp (Fig. 7F).

*Gonyaulax baltica* formed a dense, visible bloom ($4.8 \times 10^6$ cells · $L^{-1}$) in Māori Bay, New Zealand, in May, 2019. Cells from the bloom sample were 30.0–35.7 μm long (mean = 33.6 ± 1.6 μm, $n$ = 18) and 28.8–35.0 μm wide (mean = 32.1 ± 1.8 μm, $n$ = 18). The cell morphology was similar to those from South Korea, but differed in having several antapical spines as long as 6.0 μm (Fig. 8, A–F).

Living cysts from surface sediment of Māori Bay displayed an oval central body and were 33.3 μm long and 30.7 μm wide, with a small apical boss (Fig. 8G). The paracingulum descended with a displacement of twice its width (Fig. 8H).

The cyst had a wall ca. 2 μm thick ornamented with exclusively gonal, trifurcate processes 11.1–14.2 μm long (Fig. 8, G and H). There was one hypothecal petaloid trumpet-shaped process (Fig. 8I).

*Molecular phylogeny. Gonyaulax bohaiensis* strains (TIO724, 725, 726, 727, 731, LIMS-PS-3448) shared identical LSU rRNA gene sequences and differed from *G. baltica* (=*Impagidinium caspienense*, GenBank LC222302) at 42 positions (96.60% similarity), from French (GenBank MW775689), and Japanese (GenBank LC222310) *Spiniferites belerius* sequences at 72 and 86 positions (89.71% and 93.06% similarity), from *G. portimonensis* (GenBank OM228729) at 78 positions (87.74% similarity), and from *I. pallidum* (GenBank LC222304) at 297 positions (75.81% similarity). *Gonyaulax amoyensis* strains (TIO708, 709, 710, 711, 719, 722) differed from each other only at one position. They differed from *G. bohaiensis* strain TIO724 at 41 positions (96.99% similarity) and from *G. baltica* strain LIMS-PS-3408 at 92 positions (91.50% similarity). *Gonyaulax baltica* strain LIMS-PS-3408 from Korea shared identical sequences with strain CAWD374 from New Zealand and differed

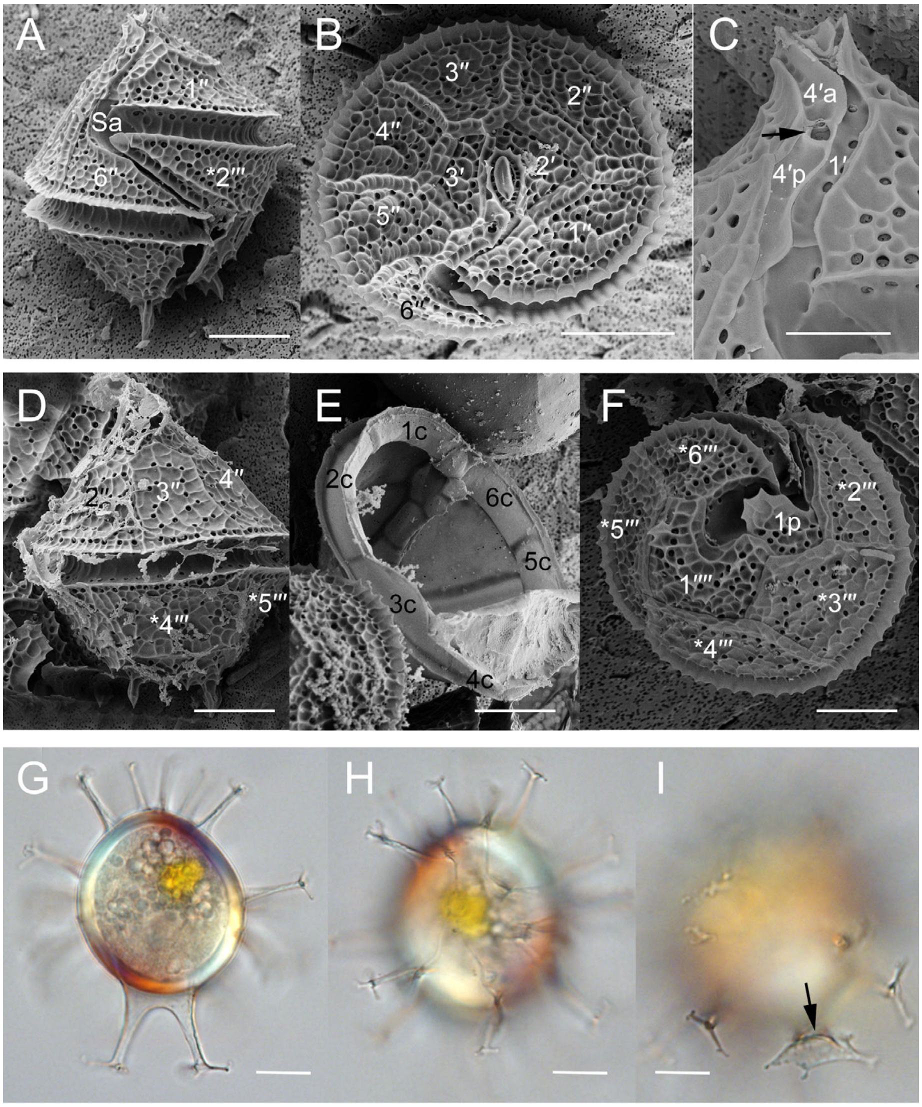


Fig. 8. Micrographs of *Gonyaulax baltica* from New Zealand. (A–F) Scanning electron microscopy. (G–I) Bright-field light microscopy. (A) Ventral view showing cingulum displacement and overhang. (B) Apical view showing six precingular (1″–6″) and two apical (2′, 3′) plates. (C) Apical view showing two apical (1′, 4′) plates, and a ventral pore (arrow). (D) Dorsal view showing three precingular (2″–4″), and two postcingular (*4‴, *5‴) plates. (E) Internal view showing six cingular plates. (F) Antapical view showing five postcingular (*2‴–*6‴) plates, one antapical plate (1⁗), and one intercalary plate (1p). (G) Mid-focus of a living cyst showing two prominent antapical processes. (H) High focus of a living cyst showing the paracinglum. (I) High focus of a living cyst showing the trumpet-shaped process (arrow). Scale bars = 10 μm, except in (C) = 5 μm. [Color figure can be viewed at wileyonlinelibrary.com]

from French and Japanese *Spiniferites belerius* sequences cited above at 83 positions and 1 position, respectively (88.09% and 99.91% similarity).

Maximum likelihood (ML) and Bayesian (BI) analyses based on LSU rRNA gene sequences yielded similar phylogenetic trees. The ML tree displayed five well-resolved clades (Fig. 9) corresponded to the families Ceratiaceae, Protoceratiaceae, Pyrophacaceae, Gonyaulacaceae, and Lingulodiniaceae. Gonyaulacaceae was monophyletic comprising the extant genus *Gonyaulax* and several fossil-based genera (*Ataxiodinium*, *Bitectatodinium*, *Impagidinium*, *Spiniferites*, and *Tectatodinium*) with maximal support (ML BS:100; BI PP: 1.0). There were two well-resolved clades (I and II) receiving strong support (100; 0.99) or maximal support. Clade I comprised *G. spinifera*, *G. polygramma*, *G. hyalina*, *G. ellegaardiae*, *G. elongata*, *G. membranacea* and related species. Clade II comprised *G. bohaiensis*, *G. amoyensis*, *G. portimonensis*, and *G. baltica*. *Impagidinium pallidum* was sister to Clade II on a long branch. *Gonyaulax baltica* comprised two ribotypes with maximal support. Ribotype A included strains from the Atlantic, whereas ribotype B included strains from the Pacific.

For SSU rRNA gene sequence comparison, *Gonyaulax amoyensis* strain TIO708 differed from *Impagidinium caspienense* (GenBank LC222300) at 40 positions (97.68% similarity), from *Spiniferites belerius*


FIG. 9. Phylogeny including *Gonyaulax bohaiensis*, *G. portimonensis* and *G. amoyensis* inferred from partial LSU rRNA (D1–D6) gene sequences using maximum likelihood (ML). New sequences are indicated in bold. Five families are labeled and marked with vertical solid lines on the right. Two clades (I and II) of Gonyaulacaceae are labeled and marked with vertical dashed line on the right. Branch lengths are drawn to scale, with the scale bar indicating the number of nucleotide substitutions per site. Numbers on branches are statistical support values for clusters to the right (left: ML bootstrap support values; right: Bayesian posterior probabilities). [Color figure can be viewed at wileyonlinelibrary.com]

(GenBank LC222309) at 69 positions (96.00% similarity), from *G. portimonensis* (OM177644) at 58 positions (96.59% similarity), from *G. baltica* strains (GenBank OM177651, OM1776512, OM1776513) at 56 positions (96.40% similarity). *Gonyaulax bohaiensis* strains TIO726 and TIO729 shared identical SSU sequences and differed from *G. amoyensis* (GenBank OM177648) at 42 positions (97.44% similarity). Maximum likelihood and BI analysis based on SSU rRNA gene sequences yielded the same results as the analyses of the LSU rRNA sequences (Fig. 10).

*Yessotoxins.* Six strains of *Gonyaulax amoyensis*, *G. baltica*, *G. bohaiensis*, and *G. portimonensis* were studied for YTXs. Very low levels of YTX were detected in the *G. bohaiensis* strain TIO732 ($0.17 \pm 0.02$ fg·cell$^{-1}$). None of the 21 other analogues were detected. YTX was not detected in the other five strains, but the limits of detection were greater than this low cell quota (Table 1) due to the limits of available biomass. Cell concentrates from bloom samples in Māori Bay and cultured cells were analyzed for YTX by LC-MS/MS. The screened analogs were YTX, homo-YTX, 45OH-YTX and 45OH-homoYTX. No trace of any of these analogues was detected.

## DISCUSSION

*Cyst-theca relationship of* Impagidinium variaseptum*,* Spiniferites pseudodelicatus *and* S. ristingensis. Previously eleven *Spiniferites* and one *Impagidinium* species have been linked to specific *Gonyaulax* species. Here, we clarify the cyst-theca relationships of *I. variaseptum* and *S. ristingensis* for the first time (Table S1). A new *Spiniferites* species, *S. pseudodelicatus* is described, and its corresponding motile cells are revealed. *Gonyaulax baltica* ribotype B is linked to *Spiniferites belerius.*

*Impagidinium variaseptum* from the Bohai Sea accords with the original description by the presence of septa of variable height and an apical boss (Marret and de Vernal 1997). Bohai Sea cysts are relatively smaller (36.0–40.5 μm long vs. 47.0–75.0 μm long) with a well-expressed paratabulation, a microgranulate wall and parasutural septa 2.0–7.6 μm high. According to Marret and de Vernal (1997), *I. variaseptum* lacks paratabulation in the sulcal area, but their plate III, Figure 5 shows a specimen that at least suggests a posterior sulcal plate. Cysts of *Impagidinium* from the Bohai Sea are morphologically similar to *I. caspienense*, but the latter has lower sutural septa (1.3–4.3 vs. 2.0–7.6 μm; Mertens et al. 2018a). Cysts of *Impagidinium* from the Bohai Sea are also morphologically similar to *I. japonicum*, but the latter lacks an apical boss and has well-developed septa as high as one third of the cyst diameter (Matsuoka 1983).

*Impagidinium variaseptum* has been reported only from recent sediments, from the Indian Ocean (Marret and de Vernal 1997), from west of Tasmania and the southwestern Pacific Ocean, and from east of New Zealand (Sun and McMinn 1994). Our findings of *I. variaseptum* in the coastal waters of Bohai Sea support its occurrence in a neritic environment, in contrast to the oceanic habitat of all other *Impagidinium* species (Marret and de Vernal 1997), except for *I. caspienense* restricted to the Caspian and Aral Seas (Zonneveld et al. 2013) also neritic habitats.

*Spiniferites ristingensis* from Portugal matches the original description of *S. ristingensis*, sharing a low apical boss, low sutural crests connecting the processes, numerous blisters and hollow undulations on the cyst surface, exclusively gonal processes with petaloid tips, and a girdle displaced with three times its widths (Head 2007). *Spiniferites ristingensis* was previously reported in the Baltic Sea of the Eemian age (ca. 127,000 years ago) when water temperatures were considered to be at least 5°C higher than at present (Head 2007). The species was reported from recent sediments of Britanny, France (Gurdebeke et al. 2018), the Black Sea and off Southwestern Portugal (Mertens et al. 2018b), from surface sediments from the West coast of Portugal (as *S. delicatus*, Ribeiro and Amorim 2008; and as *S. delicatus/ristingensis*, Ribeiro et al. 2016). It was also reported further north along the Spanish coast (the Ría de Vigo, NW Iberia), as *Spiniferites* Vigo-type cf. *S. ristringensis* (Head 2007, García-Moreiras et al. 2018).

*Spiniferites pseudodelicatus* from the East China Sea is superficially similar to *S. delicatus*, sharing a low apical boss, high sutural flanges connecting the processes, processes with petaloid tips, and a girdle displaced three times its widths (Reid 1974). However, South China Sea cysts of *S. pseudodelicatus* bear undeveloped intergonal process and are somewhat smaller (28.7–39.6 μm long) than the topotype material (40.0–60.0 μm long, Reid 1974; 36.8–50.8 μm long, Gurdebeke et al. 2018). In addition, these two species differ in wall ornamentation (Table 2). Therefore, we described a new species, *Spiniferites pseudodelicatus*. Our finding of *S. pseudodelicatus* in Xiamen Bay suggests that it prefers a neritic environment.

*Discrimination of non-fossil species.* Motile cells of *Gonyaulax bohaiensis*, *G. amoyensis*, and *G. portimonensis* are morphologically similar. All of them share a large cingulum displacement and overhang and numerous minute antapical spines. Several prominent antapical spines were reported in the *Gonyaulax spinifera* complex, such as *G. spinifera*, *G. digitale* (Kofoid 1911), *G. ellegaardiae* (Mertens et al. 2015), *G. membranacea*, and *G. elongata* (Ellegaard et al. 2003), but such spines are not observed in motile cells of *G. bohaiensis*, *G. amoyensis*, and *G. portimonensis.* In the size of antapical spines, they are much closer to *G. scrippsae*, but can be differentiated by the cingulum overhang, the number of antapical spines, and surface reticulation (Table 3).

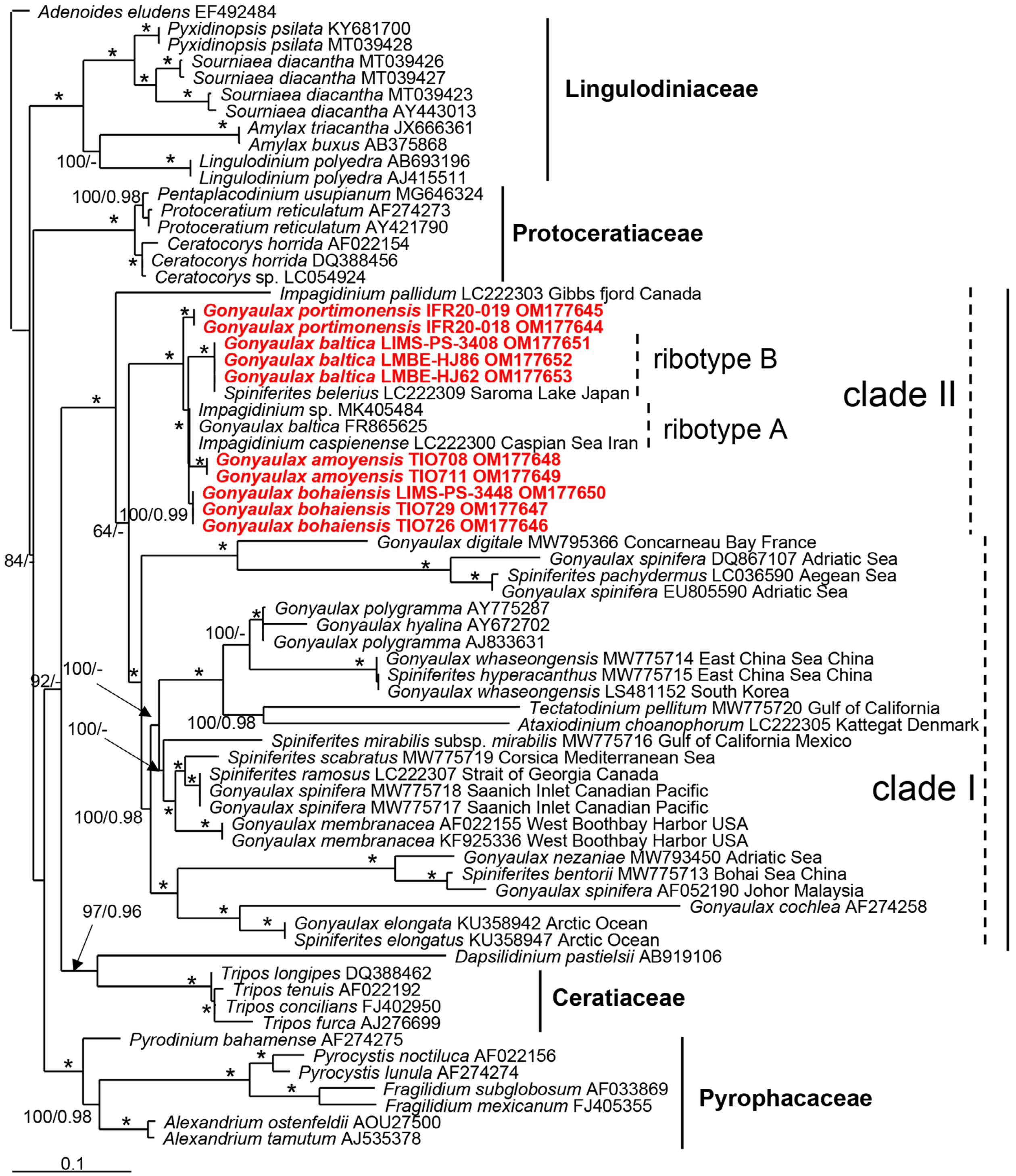


FIG. 10. Phylogeny including *Gonyaulax bohaiensis*, *G. portimonensis*, and *G. amoyensis* inferred from partial SSU rRNA gene sequences using maximum likelihood (ML). New sequences are indicated in bold. Five families are labeled and marked with vertical solid lines on the right. Two clades (I and II) of Gonyaulacaceae are labeled and marked with vertical dashed line on the right. Branch lengths are drawn to scale, with the scale bar indicating the number of nucleotide substitutions per site. Numbers on branches are statistical support values for clusters to the right (left: ML bootstrap support values; right: Bayesian posterior probabilities). [Color figure can be viewed at wileyonlinelibrary.com]

Motile cells of *Gonyaulax bohaiensis* and *G. amoyensis* are similar to *G. baltica*. All of them share a ventral pore between 4'a and 4'p, and only minor differences could be identified that do not enable unambiguous morphological identification based on the motile stage (Table 3). The ridge around apical

Table 2. Morphological comparison of fossil *Spiniferites* cysts and related species.

| Species | *S. pseudodelicatus* | *S. delicatus* | *S. ristingensis* | *S. belerius* | *S. membranaceus* | *S. mirabilis* | *Impagidinium variaseptum* | *I. caspienense* |
|---|---|---|---|---|---|---|---|---|
| Cyst length (μm) | 28.7–39.6 | 40–60 | 41.7–47.7 | 35–42 | 34–44 | 48–60 | | 34.0–39.3 |
| Cyst width (μm) | 26.2–35.6 | 35–54 | 31.9–38.3 | 28–37 | 34–43 | 44–58 | | 26.8–31.7 |
| Apical boss | low | low | low | low | Clear | Absent | Present | Present |
| Petaloid processes | Present | Present | Present | An antapical trumpet shaped process | Absent | Absent | Absent | Absent |
| Membranous flanges | Low to mid-high | High | Low to high | High | Antapical flange | Antapical flange | low to mid-high | Low |
| Processes | Occasional intergonal | Exclusively gonal | Exclusively gonal | Exclusively gonal | Exclusively gonal | Consistent intergonal | Exclusively gonal, minute furcations | None |
| Process length/septa height | 5.6–12.9 μm | 21–29 μm | 11.5–14.0 μm | 7–15 μm | 12–17 μm | 10.4–21.0 μm | 2.0–7.6 μm | 1.3–4.3 μm |
| Ventral pore | Absent | Absent | Absent | Absent | Absent | Absent | Present | Present |
| Cingulum displacement | Two-three cingular widths | Three cingular widths | Three cingular widths | One to three cingular widths | Two cingular widths | Three cingular widths | Two to three cingular widths | 2.5–2.7 widths |
| Cyst wall ornamentation | Microgranulate | Microgranular to microreticulate | small blisters and hollow undulations | Smooth | Microgranular to micropunctate | Ruptured or folded with a distinct microgranular surface | Microgranulate with parasutural crests | Finely granulate |
| Archeopyle | Reduced | Reduced | Not reduced | Not reduced | Reduced | Reduced | Reduced | Not reduced |
| References | Present study | Reid (1974), Gurdebeke et al. (2018) | Present study | Reid (1974), Gurdebeke et al. (2018) | Reid (1974), Gurdebeke et al. (2018) | Reid (1974) | Present study | Mertens et al. (2018a) |

TABLE 3. Comparison of motile cells of *Gonyaulax bohaiensis*, *G. amoyensis*, *G. portimonensis*, and some related species.

| Species | *G. bohaiensis* | *G. amoyensis* | *G. portimonensis* | *G. baltica* ribotype B | *G. baltica* ribotype A | *G. scrippsae* |
|---|---|---|---|---|---|---|
| Cell length (μm) | 25.3–45.6 | 23.8–42.4 | 30.0–42.9 | 27.6–44.5 | 31–37 | 29-39 |
| Cell width (μm) | 21.1–37.0 | 19.2–29.1 | 24.4–38.6 | 23.0–34.9 | 27–32 | 27-34 |
| Shoulders | Intermediate | Intermediate | Intermediate | Intermediate | Intermediate | NA |
| Reticulation | Pronounced | Pronounced | Pronounced and dense | Pronounced | Pronounced | Fine, subparallel lines |
| Pores | Many | Many | Many | Many | Few-many | Few |
| Ventral pore | Present | Present | Present | Present | Present | Present |
| Cingulum | | | | | | |
| Reticulation | Striated | Striated | Striated | Striated | Striated | Vertical ribs |
| Width (μm) | 3.0–4.5 | 2.2–4.0 | 3.0–4.3 | 2.5–3.5 | 3.0–4.0 | |
| Displacement | 2.4–2.8 | 2.0–3.0 | 1.8–3.0 | 2.5–3.5 | 2.5–4.5 | 2.0–3.0 |
| Overhang | 2.0–2.8 | 1.8–2.5 | 1.4–2.7 | 2.0–3.0 | 2.0–3.3 | 0.1–1.0 |
| Angle (in degrees) | 35–45 | 25–35 | 25–40 | 40–45 | 23–45 | NA |
| Sulcus | | | | | | |
| Widening | No | No | No | No | No | Yes |
| Sa, anteriorly | Broad | Broad | Broad | Broad | Broad | NA |
| 4′a plate | Separated, small | Separated, small | Separated, intermediate | Separated, small | Separated, small | NA |
| Apical horn | Short | Short | Short | Short | Short | Short |
| Apical pore complex | Smooth | Smooth | Smooth | Smooth | Smooth | NA |
| Ridge around APC | High | Low | Low | Intermediate | Low, scalloped | NA |
| Antapical spines | Minute, 10–26 | Minute, 2–18 | Intermediate, 2–4, one larger right | Minute, 11–18 | Small, 0–10 | Minute, 0–2 |
| References | Present study | Present study | Present study | Present study | Ellegaard et al. (2002) | Kofoid (1911) |

NA, not available.

pore complex is high in *G. bohaiensis*, but low in *G. amoyensis* and *G. baltica*. *Gonyaulax portimonensis* has a relatively larger antapical spine in the right side but in other three species the antapical spines are equal in length. *Gonyaulax portimonensis* resembles *G. monacantha* (Pavillard 1916), but is smaller (30.0–42.9 vs. 45–55 μm long). *Gonyaulax portimonensis* also resembles *G. cochlea* (Meunier 1919) but has a larger cingulum displacement (2.0 cingulum width vs. 1.0). Based on morphological characteristics from both motile stages and cysts, we proposed *G. bohaiensis* as the motile stage of *I. variaseptum*, and *G. amoyensis* and *G. portimonensis* corresponding to cysts resembling *S. pseudodelicatus* and *S. ristingensis*, respectively. On the other hand, *G. baltica* is able to produce cysts resembling *I. caspienense* and *S. belerius* (Mertens et al. 2018a, present study).

The *Gonyaulax baltica* strain LIMS-PS-3408 from Korea and a bloom sample of *Gonyaulax baltica* from New Zealand are indistinguishable from the type material in morphology, but genetically separated from *G. baltica* of the Baltic Sea. The number and length of antapical spines appear slightly plastic in *G. baltica* ribotype A, for example, strains from the Caspian Sea show numerous minute spines ca 1.0 μm long (Mertens et al. 2018a), but can be 2.0 μm long in cells from the Baltic Sea (Ellegaard et al. 2002). Similar variation was also observed in *G. baltica* ribotype B; strains from South Korea show numerous minute spines but the bloom sample from New Zealand show longer and fewer spines.

*Molecular phylogenetics.* Our molecular phylogenies, based on LSU and SSU rRNA gene sequences, are congruent and both support the monophyly of the extant genus *Gonyaulax*, but indicate two clades within the genus. Clade I includes *G. spinifera* like species with two prominent antapical spines, such as *G. digitale*, *G. membranacea*, *G. elongata*, *G. ellegaardiae*, *G. nezaniae* as well as those without spines, such as *G. hyalina*. In contrast, Clade II includes *G. baltica* like species with relatively short and numerous antapical spines, as also observed in *G. bohaiensis*, *G. amoyensis*, and *G. portimonensis*. Kofoid (1911) proposed the subgenus *Gonyaulax* that was defined to include species with spheroidal or polyhedral cells, Therefore, species of both Clades I and II can be classified within this subgenus, but the subgenus appears polyphyletic. DNA sequences of subgenera *Acanthogonyaulax* and *Fusigonyaulax*, characterized by an elongated apical and one or two antapical horns (Kofoid 1911), are not available. The subgenus *Steiniella* includes *G. fragilis* and *G. hyalina* (Carbonell-Moore and Mertens 2019); however, *G. hyalina* is also nested within Clade I. One subgenus for Clade I and another for Clade II could be recognized based on the number, size of antapical spines in motile cells, or the shape of processes in cysts.

The neritic *Impagidinium caspienense* and *I. variaseptum* (as *Gonyaulax bohaiensis*) are in the same clade (Clade II), while oceanic *I. pallidum* is sister to Clades II on a long branch (Figs. 9, 10). Currently, DNA sequences of extant oceanic *I. japonicum*, *I.*

*paradoxum*, *I. patulum*, and *I. aculeatum*, *I. plicatum*, *I. sphaericum*, and *Impagidinium velorum* are not available. It will be interesting to see if the morphological criteria like the shape of plate 6″, height of septa and presence/absence of an apical boss might support the split of *Impagidinium* into one genus for neritic species and another for oceanic species.

The grouping of *Spiniferites pseudodelicatus*, *S. ristingensis*, and *S. belerius* in the same clade with *Impagidinium* instead of with other *Spiniferites* species challenges the current taxonomic criteria based on morpho-anatomy. *Spiniferites pseudodelicatus* and *S. ristingensis* share high flanges that connect the processes as also observed in *I. variaseptum* and *I. caspienense* (Gurdebeke et al. 2018, Mertens et al. 2018a). Reduced process length in cysts of *Gonyaulax baltica/I. caspienense* was attributed to low salinity as demonstrated in culture experiments and a field survey (Dale 1996, Ellegaard et al. 2002). However, the short processes in *I. variaseptum* appear not to be related with low salinity as they were found in seawater with typical salinity values. *Spiniferites membranaceus* and *S. mirabilis* also have a high flange, but it is only present in the antapical plate. The fact that *S. mirabilis* is sister to S. *membranaceus* in the SSU rRNA gene based phylogeny (Fig. 10) suggests that this character might be taxonomically significant as well.

Petaloid processes appear to be characteristic of cysts produced by *Gonyaulax baltica* and related species, as observed in *Spiniferites pseudodelicatus*, *S. ristingensis*, *S. belerius* (Mertens et al. 2018a) and in cysts produced in cultures of *G. baltica* (Ellegaard et al. 2002), suggesting that this trait is phylogenetically significant. *Spiniferites delicatus* also has petaloid processes (Reid 1974) and needs to be sequenced to see if it is in the same clade as *G. baltica*.

Our findings reveal two ribotypes of *Gonyaulax baltica* as well as the first record of a bloom by this species. Ribotype B of *G. baltica* from the Pacific cannot be differentiated morphologically from ribotype A in the Atlantic, suggesting that this is a cryptic species. Whether ribotype B is able to generate *Impagidinium* like cysts in low salinity as ribotype A does remain to be determined. The low genetic similarity between the two ribotypes of *G. baltica* (around 88%) is comparable to *Sourniaea diacantha* (86%), which also shows two ribotypes of Atlantic and Pacific origin (Zhang et al. 2020).

*Yessotoxin production.* The finding of a very low YTX cell quota of *Gonyaulax bohaiensis* strain TIO732 is noteworthy, even though no YTX was detected in the other two strains (TIO726 and TIO711). The detection limits of these two measurements (1.34 and 0.4 fg $\cdot$ cell$^{-1}$, respectively) were above the YTX cell quota of strain TIO732 (0.17 fg $\cdot$ cell$^{-1}$) due to lower biomass and the use of a different instrument. For this reason, the lack of YTX detection in strains TIO726 and TIO711 does not necessarily indicate its absence. YTX production has been well documented in the *G. spinifera* group (*G. membranacea* and *G. ellegaardiae*; Chikwililwa et al. 2019, Pitcher et al. 2019), but our results suggest that YTX production may also occur in the *G. baltica* clade, even though there are not many records.

*Dinoflagellate nomenclature.* The International Code of Nomenclature for algae, fungi and plants (ICN, Turland et al. 2018) sanctions the use of dual nomenclature: It allows fossil- and non-fossil taxa to have separate names even if they are linked. This dual nomenclature system has been applied to dinoflagellates for decades. Attribution of living dinoflagellate cysts to motile stages have been investigated intensively (Wall 1967, Wall and Dale 1967, Ellegaard et al. 2003, Mertens et al. 2015, Gu et al. 2021). However, there remain many unresolved issues, especially for those living “fossil” cysts such as *Spiniferites*. Here, we relate several new *Gonyaulax* species with resting stages resembling *Impagidinium variaseptum*, *Spiniferites pseudodelicatus* and *S. ristingensis*, respectively. Future work should contribute to the unification of nomenclature, but clearly there is still much work to be done before this can be achieved. Therefore, in the present work, we chose to use the dual nomenclature.

This work was supported by the National Natural Science Foundation of China (grants 42076085, 42030404), the National Marine Biodiversity Institute of Korea (grant 2021M01100), the KRIBB Research Initiative Program (grant KGM5232113) and a National Research Foundation of Korea grant (MSIT) (2021R1C1C1008377). The Regional Council of Brittany, the General Council of Finistère and the urban community of Concarneau-Cornouaille-Agglomération are acknowledged for the funding of the Sigma 300 FE-SEM of the station of Marine Biology in Concarneau. KNM, VS, AA, and PH acknowledge the project H2020 RISE project EMERTOX—Emergent Marine Toxins in the North Atlantic and Mediterranean: New Approaches to Assess their Occurrence and Future Scenarios in the Framework of Global Environmental Changes—Grant Agreement No. 778069. LM and KFS acknowledge the Seafood Safety Research Platform funded by the New Zealand Ministry for Business, Innovation and Employment (Contract CAWX1801) and a Royal Society of New Zealand Catalyst: Seeding Grant (CSG-CAW1601) to KS and KNM. AA acknowledges funding through National Science Foundation of Portugal (FCT, I.P.) under the project UID/MAR/04292/2020. We thank Paul Gabrielson for detailed edits.

## AUTHOR CONTRIBUTIONS

**H. Gu:** Conceptualization (lead); Data curation (equal); Formal analysis (equal); Funding acquisition (equal); Investigation (equal); Methodology (equal); Project administration (lead); Resources (equal); Software (equal); Supervision (equal); Validation (equal); Visualization (equal); Writing – original draft (equal); Writing – review & editing (equal). **K.N. Mertens:** Conceptualization (equal); Formal analysis (equal); Investigation (equal); Methodology (equal); Writing – review & editing (equal). **A. Derrien:** Data curation (equal); Formal analysis (equal); Investigation (equal); Methodology (equal); Writing – review & editing (equal). **G. Bilien:** Data curation (equal); Formal analysis (equal); Investigation (equal); Methodology (equal); Writing – review & editing (equal). **Z. Li:** Data curation (equal); Formal analysis (equal); Investigation (equal); Methodology (equal); Writing – review & editing (equal). **P. Hess:** Data curation (equal); Formal analysis (equal); Investigation (equal); Methodology (equal); Writing – review & editing (equal). **V. Séchet:** Data curation (equal); Formal analysis (equal); Investigation (equal); Methodology (equal). **B. Krock:** Data curation (equal); Formal analysis (equal); Investigation (equal); Methodology (equal); Writing – review & editing (equal). **A. Amorim:** Data curation (equal); Formal analysis (equal); Investigation (equal); Methodology (equal); Writing – review & editing (equal). **Z. Li:** Data curation (equal); Formal analysis (equal); Investigation (equal); Methodology (equal); Writing – review & editing (equal). **V. Pospelova:** Data curation (equal); Formal analysis (equal); Investigation (equal); Methodology (equal); Writing – review & editing (equal). **K.F. Smith:** Data curation (equal); Formal analysis (equal); Investigation (equal); Methodology (equal); Writing – review & editing (equal). **L. Mackenzie:** Data curation (equal); Formal analysis (equal); Investigation (equal); Methodology (equal); Writing – review & editing (equal). **J.Y. Yoon:** Data curation (equal); Formal analysis (equal); Investigation (equal); Methodology (equal). **H.J. Kim:** Data curation (equal); Formal analysis (equal); Investigation (equal); Methodology (equal). **H.H. Shin:** Conceptualization (equal); Data curation (equal); Formal analysis (equal); Funding acquisition (equal); Investigation (equal); Methodology (equal); Project administration (equal); Supervision (equal); Writing – review & editing (equal).


Álvarez, G., Uribe, E., Regueiro, J., Blanco, J. & Fraga, S. 2016. *Gonyaulax taylorii*, a new yessotoxins-producer dinoflagellate species from Chilean waters. *Harmful Algae* 58:8–15.

Balech, E. 1980. On the thecal morphology of dinoflagellates with special emphasis on circular and sulcal plates. *Anales Del Centro De Ciencias Del Mar Y Limnologia, Universidad Nacional Autonomia De Mexico* 7:57–68.

Boc, A., Diallo, A. B. & Makarenkov, V. 2012. T-REX: a web server for inferring, validating and visualizing phylogenetic trees and networks. *Nucleic Acids Res.* 40:W573–9.

Bolch, C. 1997. The use of sodium polytungstate for the separation and concentration of living dinoflagellate cysts from marine sediments. *Phycologia* 36:472–8.

Carbonell-Moore, M. C. & Mertens, K. N. 2019. Should *Gonyaulax hyalina* and *Gonyaulax fragilis* (Dinophyceae) remain two different taxa? *Phycologia* 58:685–9.

Chikwililwa, C., McCarron, P., Waniek, J. J. & Schulz-Bull, D. E. 2019. Phylogenetic analysis and yessotoxin profiles of *Gonyaulax spinifera* cultures from the Benguela Current upwelling system. *Harmful Algae* 85:101626.

Chomérat, N. & Couté, A. 2008. *Protoperidinium bolmonense* sp. nov. (Peridiniales, Dinophyceae), a small dinoflagellate from a brackish hypereutrophic lagoon (South of France). *Phycologia* 47:392–403.

Dale, B. 1983. Dinoflagellate resting cysts: “benthic plankton”. *In* Fryxell, G. A. [Ed.], *Survival Strategies of the Algae*. Cambridge University Press, Cambridge, UK, pp. 69–136.

Dale, B. 1996. Dinoflagellate cyst ecology: modeling and geological applications. *In* Jansonius, J. & McGregor, D. C. [Eds.] *Palynology: Principles and Applications*. American Association of Stratigraphic Palynologists Foundation, Dallas, TX, pp 1249–75.

Deflandre, G. & Cookson, I. C. 1955. Fossil microplankton from Australian late Mesozoic and Tertiary sediments. *Mar. Freshw. Res.* 6:242–314.

Diesing, K. M. 1866. Revision der Prothelminthen. Abtheilung: Mastigophoren. Sitzungsberichte der Kaiserlichen Akademie der Wissenschaften. Mathematisch-Naturwissenschaftliche Classe. Abt. 1. *Mineralogie, Botanik, Zoologie, Anatomie, Geologie Und Palaontologie* 52:287–401.

Dodge, J. 1989. Some revisions of the family Gonyaulacaceae (Dinophyceae) based on a scanning electron microscope study. *Bot. Mar.* 32:275–98.

Ellegaard, M., Daugbjerg, N., Rochon, A., Lewis, J. & Harding, I. 2003. Morphological and LSU rDNA sequence variation within the *Gonyaulax spinifera-Spiniferites* group (Dinophyceae) and proposal of *G. elongata* comb. nov. and *G. membranacea* comb. nov. *Phycologia* 42:151–64.

Ellegaard, M., Lewis, J. & Harding, I. C. 2002. Cyst-theca relationship, life cycle, and effects of temperature and salinity on the cyst morphology of *Gonyaulax baltica* sp. nov. (Dinophyceae) from the Baltic Sea area. *J. Phycol.* 38:775–89.

Evitt, W. R. 1963. A discussion and proposals concerning fossil dinoflagellates, hystrichospheres, and acritarchs, I. *Proc. Natl. Acad. Sci. USA* 49:158–64.

Fensome, R. A., Taylor, F. J. R., Norris, G., Sarjeant, W. A. S., Wharton, D. I. & Williams, G. L. 1993. A classification of fossil and living dinoflagellates. *Micropaleontology Special Publication* 7:1–245.

García-Moreiras, I., Pospelova, V., García-Gil, S. & Sobrino, C. M. 2018. Climatic and anthropogenic impacts on the Ría de Vigo (NW Iberia) over the last two centuries: a high-resolution dinoflagellate cyst sedimentary record. *Palaeogeogr. Palaeoclimatol. Palaeoecol.* 504:201–18.

Gómez, F. 2012. A checklist and classification of living dinoflagellates (Dinoflagellata, Alveolata). *CICIMAR Oceánides* 27:65–140.

Gu, H., Huo, K., Krock, B., Bilien, G., Pospelova, V., Li, Z., Carbonell-Moore, C., Morquecho, L., Ninčević, Ž. & Mertens, K. N. 2021. Cyst-theca relationships of *Spiniferites bentorii*, *S. hyperacanthus*, *S. ramosus*, *S. scabratus* and molecular phylogenetics of *Spiniferites* and *Tectatodinium* (Gonyaulacales, Dinophyceae). *Phycologia* 60:332–53.

Guillard, R. R. L. & Ryther, J. H. 1962. Studies of marine planktonic diatoms. I. *Cyclotella nana* Hustedt and *Detonula confervacea* Cleve. *Can. J. Microbiol.* 8:229–39.

Gurdebeke, P. R., Mertens, K. N., Bogus, K., Marret, F., Chomérat, N., Vrielinck, H. & Louwye, S. 2018. Taxonomic re-investigation and geochemical characterization of Reid’s (1974) species of *Spiniferites* from holotype and topotype material. *Palynology* 42:93–110.

Hall, T. A. 1999. BioEdit: a user-friendly biological sequence alignment editor and analysis program for Windows 95/98/NT. *Nucleic Acids Symp. Ser.* 41:95–8.

Head, M. J. 2007. Last Interglacial (Eemian) hydrographic conditions in the southwestern Baltic Sea based on dinoflagellate cysts from Ristinge Klint. *Denmark. Geol. Mag.* 144:987–1013.

Katoh, K. & Standley, D. M. 2013. MAFFT multiple sequence alignment software version 7: improvements in performance and usability. *Mol. Biol. Evol.* 30:772–80.

Kofoid, C. A. 1911. Dinoflagellata of the San Diego region, IV. The genus *Gonyaulax* with notes on its skeletal morphology and a discussion of its generic and specific characters. *U. Calif. Pub. Zool.* 8:187–286.

Lewis, J., Rochon, A. & Harding, I. 1999. Preliminary observations of cyst-theca relationships in *Spiniferites ramosus* and *Spiniferites membranaceus* (Dinophyceae). *Grana* 38:113–24.

Lim, A. S., Jeong, H. J., Kwon, J. E., Lee, S. Y. & Kim, J. H. 2018. *Gonyaulax whaseongensis* sp. nov. (Gonyaulacales, Dinophyceae), a new phototrophic species from Korean coastal waters. *J. Phycol.* 54:923–8.

Luo, Z., Mertens, K. N., Nézan, E., Gu, L., Pospelova, V., Thoha, H. & Gu, H. 2019. Morphology, ultrastructure and molecular phylogeny of cyst-producing *Caladoa arcachonensis* gen. et sp. nov. (Peridiniales, Dinophyceae) from France and Indonesia. *Eur. J. Phycol.* 54:235–48.

Marret, F. & de Vernal, A. 1997. Dinoflagellate cyst distribution in surface sediments of the southern Indian Ocean. *Mar. Micropaleontol.* 29:367–92.

Matsuoka, K. 1983. Late Cenozoic dinoflagellates and acritarchs in the Niigata district, central Japan. *Palaeontogr. Abt. B Paläophytologie* 187:89–154.

Mertens, K. N., Aydin, H., Uzar, S., Takano, Y., Yamaguchi, A. & Matsuoka, K. 2015. Relationship between the dinoflagellate cyst *Spiniferites pachydermus* and *Gonyaulax ellegaardiae* sp. nov. from Izmir Bay, Turkey, and molecular characterization. *J. Phycol.* 51:560–73.

Mertens, K. N. & Carbonell-Moore, C. 2018. Introduction to *Spiniferites* Mantell 1850 special issue. *Palynology* 42:1–9.

Mertens, K. N., Takano, Y., Gu, H., Bagheri, S., Pospelova, V., Pieńkowski, A. J., Leroy, S. & Matsuoka, K. 2018a. Cyst-theca relationship and phylogenetic position of *Impagidinium caspienense* incubated from Caspian Sea surface sediments: relation to *Gonyaulax baltica* and evidence for heterospory within Gonyaulacoid dinoflagellates. *J. Eukaryot. Microbiol.* 64:829–42.

Mertens, K. N., Van Nieuwenhove, N., Gurdebeke, P. R., Aydin, H., Bogus, K., Bringué, M., Dale, B., De Schepper, S., de Vernal, A. & Ellegaard, M. 2018b. The dinoflagellate cyst genera *Achomosphaera* Evitt 1963 and *Spiniferites* Mantell 1850 in Pliocene to modern sediments: a summary of round table discussions. *Palynology* 42:10–44.

Meunier, A. 1919. Microplankton de la mer Flamande. III. Les Péridiniens. *Le Musée royal d'histoire naturelle de Belgique, Mémoires* 8:3–116.

Nézan, E., Tillmann, U., Bilien, G., Boulben, S., Chèze, K., Zentz, F., Salas, R. & Chomérat, N. 2012. Taxonomic revision of the dinoflagellate *Amphidoma caudata*: transfer to the genus *Azadinium* (Dinophyceae) and proposal of two varieties, based on morphological and molecular phylogenetic analyses. *J. Phycol.* 48:925–39.

Pavillard, J. 1916. Recherches sur les Péridiniens du Golfe du Lion. *Institut De Botanique De L'université De Montpellier Et De La Station Zoologique De Cette, Travail, Série Mixte, Mémoire* 4:1–73.

Pitcher, G. C., Foord, C. J., Macey, B. M., Mansfield, L., Mouton, A., Smith, M. E., Osmond, S. J. & van der Molen, L. 2019. Devastating farmed abalone mortalities attributed to yessotoxin-producing dinoflagellates. *Harmful Algae* 81:30–41.

Posada, D. 2008. jModelTest: phylogenetic model averaging. *Mol. Biol. Evol.* 25:1253–6.

Reid, P. 1974. Gonyaulacacean dinoflagellate cysts from the British Isles. *Nova Hedwig* 25:579–637.

Rhodes, L., McNabb, P., De Salas, M., Briggs, L., Beuzenberg, V. & Gladstone, M. 2006. Yessotoxin production by *Gonyaulax spinifera*. *Harmful Algae* 5:148–55.

Ribeiro, S. & Amorim, A. 2008. Environmental drivers of temporal succession in recent dinoflagellate cyst assemblages from a coastal site in the North-East Atlantic (Lisbon Bay, Portugal). *Mar. Micropaleontol.* 68:156–78.

Ribeiro, S., Amorim, A., Abrantes, F. & Ellegaard, M. 2016. Environmental change in the Western Iberia upwelling ecosystem since the preindustrial period revealed by dinoflagellate cyst records. *Holocene* 26:874–89.

Riccardi, M., Guerrini, F., Roncarati, F., Milandri, A., Cangini, M., Pigozzi, S., Riccardi, E. et al. 2009. *Gonyaulax spinifera* from the Adriatic sea: toxin production and phylogenetic analysis. *Harmful Algae* 8:279–90.

Rochon, A., Lewis, J., Ellegaard, M. & Harding, I. C. 2009. The *Gonyaulax spinifera* (Dinophyceae) "complex": perpetuating the paradox? *Rev. Palaeobot. Palynol.* 155:52–60.

Ronquist, F. & Huelsenbeck, J. P. 2003. MrBayes 3: Bayesian phylogenetic inference under mixed models. *Bioinformatics* 19:1572–4.

Smith, K. F., Rhodes, L., Verma, A., Curley, B. G., Harwood, D. T., Kohli, G. S., Solomona, D., Rongo, T., Munday, R. & Murray, S. A. 2016. A new *Gambierdiscus* species (Dinophyceae) from Rarotonga, Cook Islands: *Gambierdiscus cheloniae* sp. nov. *Harmful Algae* 60:45–56.

Stamatakis, A., Hoover, P. & Rougemont, J. 2008. A rapid bootstrap algorithm for the RAxML Web servers. *Syst. Biol.* 57:758–71.

Stover, L. E. & Evitt, W. R. 1978. *Analyses of Pre-Pleistocene Organic-Walled Dinoflagellates.* Stanford University Publication, Stanford, CA, USA, 299 pp.

Sun, X. & McMinn, A. 1994. Recent dinoflagellate cyst distribution associated with the Subtropical Convergence on the Chatham Rise, east of New Zealand. *Mar. Micropaleontol.* 23:345–56.

Takano, Y. & Horiguchi, T. 2006. Acquiring scanning electron microscopical, light microscopical and multiple gene sequence data from a single dinoflagellate cell. *J. Phycol.* 42:251–6.

Thiers, B. M. 2022. Index Herbariorum. http://sweetgum.nybg.org/science/ih/

Turland, N. J., Wiersema, J. H., Barrie, F. R., Greuter, W., Hawksworth, D. L., Herendeen, P. S., Knapp, S., Kusber, W. H., Li, D. Z. & Marhold, K. et al. 2018. International Code of Nomenclature for algae, fungi, and plants (Shenzhen Code) adopted by the Nineteenth International Botanical Congress Shenzhen, China, July 2017. Regnum Vegetabile 159. Glashütten: Koeltz Botanical Books. https://doi.org/10.12705/Code.2018

Wall, D. 1967. Fossil microplankton in deep-sea cores from the Caribbean Sea. *Palaeontology* 10:95–123.

Wall, D. & Dale, B. 1967. The resting cysts of modern marine dinoflagellates and their palaeontological significance. *Rev. Palaeobot. Palynol.* 2:349–54.

Wang, N., Mertens, K. N., Krock, B., Luo, Z., Derrien, A., Pospelova, V., Liang, Y. et al. 2019. Cryptic speciation in *Protoceratium reticulatum* (Dinophyceae): evidence from morphological, molecular and ecophysiological data. *Harmful Algae* 88:101610.

Williams, G. L., Fensome, R. A. & MacRae, R. A. 2017. DINOFLAJ3. American association of stratigraphic palynologists, data series no. 2. http://dinoflaj.smu.ca/dinoflaj3

Yamaguchi, A. & Horiguchi, T. 2005. Molecular phylogenetic study of the heterotrophic dinoflagellate genus *Protoperidinium* (Dinophyceae) inferred from small subunit rRNA gene sequences. *Phycol. Res.* 53:30–42.

Zhang, W., Li, Z., Mertens, K. N., Derrien, A., Pospelova, V., Carbonell-Moore, M. C., Bagheri, S., Matsuoka, K., Shin, H. H. & Gu, H. 2020. Reclassification of *Gonyaulax verior* (Gonyaulacales, Dinophyceae) as *Sourniaea diacantha* gen. et comb. nov. *Phycologia* 59:246–60.

Zonneveld, K. A. F., Marret, F., Versteegh, G. J. M., Bogus, K., Bonnet, S., Bouimetarhan, I., Crouch, E. et al. 2013. Atlas of modern dinoflagellate cyst distribution based on 2405 data points. *Rev. Palaeobot. Palynol.* 191:1–197.

Zorzi, C., Head, M. J., Matthiessen, J. & de Vernal, A. 2019. *Impagidinium detroitense* and *I.? diaphanum*: two new dinoflagellate cyst species from the Pliocene of the North Pacific Ocean, and their biostratigraphic significance. *Rev. Palaeobot. Palynol.* 264:24–37.

**Supporting Information**

Additional Supporting Information may be found in the online version of this article at the publisher's web site:

**Figure S1**. Micrographs of *Gonyaulax bohaiensis* strain TIO726 from Bohai Sea, China. (A–D, F) Bright-field light microscopy. (E) Epifluorescence. (A) The living cyst yielding strain TIO726 showing the nucleus (N). (B) The empty cyst yielding strain TIO726 showing the operculum. (C) Ventral view of a living cell showing the cingulum displacement and overhang. (D) Dorsal view of a living cell showing a nucleus (N) and numerous chloroplasts. (E) Ventral view of a SYBR Green stained cell showing the elongated nucleus (N). (F) The theca of a living cell showing the ventral pore (arrow). Scale bars = 10 μm.

**Figure S2**. Schematic drawings of *Gonyaulax bohaiensis*. (A) Ventral view. (B) Dorsal view. (C) Apical view. (D) Antapical view.

**Figure S3**. Scanning electron micrographs of *Gonyaulax bohaiensis* strain LIMS-PS-3448 from Korea. (A) Ventral view showing cingulum displacement and overhang. (B) Dorsal view showing three precingular (2″–4″), and three postcingular (*3‴–*5‴) plates. (C) Apical-ventral view showing the first and fourth apical plates (1′, 4′) and a ventral pore (arrow). (D) Apical view showing five precingular (1″–5″), and two apical (2′, 3′) plates. (E) Antapical view showing five postcingular (*2‴–*6‴) plates, one antapical plate (1⁗) and one intercalary plate (1p). Scale bars = 5 μm.

**Figure S4**. Light micrographs of *Gonyaulax amoyensis* strain TIO711 from Xiamen Bay, China. (A) Ventral view of a living cell showing the cingulum displacement and overhang. (B) Dorsal view of a living cell showing a nucleus (N) and numerous chloroplasts. (C, D) Ventral view of SYBR Green stained cells showing the elongated nucleus (N). Scale bars = 10 μm.

**Figure S5**. Schematic drawings of *Gonyaulax amoyensis*. (A) Ventral view. (B) Dorsal view. (C) Apical view. (D) Antapical view.

**Figure S6**. Light micrographs of *Gonyaulax portimonensis*. (A) Ventral view of an empty theca show cingulum displacement and overhang. (B, C) High and mid-focus of living cells showing the chloroplasts and nucleus. (D) Ventral view of an empty theca showing the ventral pore (arrow).

**Figure S7**. Schematic drawings of *Gonyaulax portimonensis*. (A) Ventral view. (B) Dorsal view. (C) Apical view. (D) Antapical view.

**Figure S8**. Light micrographs of *Gonyaulax baltica* strain LIMS-PS-3408 from South Korea. (A) Mid-focus of a living cell showing intermediate shoulders. (B) Dorsal view of a living cell showing numerous chloroplasts. (C) Ventral view of a living cell showing the cingulum displacement and overhang. (D) Dorsal view of a living cell showing an elongated nucleus (N). (E, F) Ventral view of SYBR Green stained cells showing the curved nucleus (N). Scale bars = 10 μm.

**Table S1**. Confirmed cyst–theca relationship of *Spiniferites* and related species.

**Table S2**. Mass transitions of the selected reaction monitoring (SRM) LC-MS/MS experiments and their respective YTX designations cited in Sala-Pérez et al. (2016). All compounds and entries refer to original numbering in Miles et al. (2005a,b).

**Table S3**. Mass transitions of the multiple reaction monitoring (MRM) LC-MS/MS experiments.